FLOW AND FRACTURE OF METALS UNDER COMPLEX STRESS

R. M. Haythornthwaite
D. R. Jenkins
M. D. Coon
C. K. Felber

FOREWORD

This report was prepared by the Department of Engineering Mechanics, College of Engineering, The University of Michigan, Ann Arbor, Michigan, under Contract No. AF 33(615)-1572. The contract was initiated under Project No. 7353, "Characterization of Solid Phase and Interphase Phenomena in Crystalline Substances," Task No. 735301, "Mechanical Metallurgy." The work was administered by the Advanced Metallurgical Studies Branch, Metals and Ceramics Division, Air Force Materials Laboratory, Research and Technology Division, Air Force Systems Command, Wright-Patterson Air Force Base, Ohio, Dr. A. J. Herzog, Project Engineer.

The report is presented in two parts, Part I "Analysis of Complex Stress States in the Tube Test," by R. M. Haythornthwaite, and Part II "Effects of Prestrain on Plastic Flow and Fracture in a Steel Subject to Complex Stress," by R. M. Haythornthwaite, D. R. Jenkins, M. D. Coon, and C. K. Felber.

This is a final summary report and describes the research conducted during the period 3 March 1964 to 30 September 1965. The manuscript was released by the authors in May, 1966 for publication as an RTD Technical Report.

F. R. BONANNO, Major, USAF
Chief, Advanced Metallurgical Studies
Branch
Metals and Ceramics Division
AF Materials Laboratory

ABSTRACT

The effects of severe initial prestrain on the response of a steel to complex stress states is investigated in a series of tube tests. The steel becomes highly anisotropic, with a pronounced Bauschinger effect, so far as the resumption of plastic flow is concerned. A detailed analysis of the subsequent history of hardening shows that, in the later stages of plastic flow, it may be possible to simulate the behavior of the material with reasonable accuracy by means of an isotropic rigid-plastic model. Even after substantial prestrains (plastic effective strain, 0.03) sufficient ductility remains to allow the redistribution of loads necessary for an ultimate strength (plastic) analysis of components.

In Part I of the report a relatively complete study is made on the basis of plastic theory and it is shown that the stress distribution may be highly nonuniform even in a very thin cylinder; moreover the distribution is dependent on the nature of the yield criterion and so cannot be known in advance. This circumstance renders the calculation of "average" stresses of limited value and it is better to deal directly with the applied tractions, a procedure which is adopted in the remainder of the report.

Part II presents details of the series of tests on tubes subject to various combinations of internal pressure and a tensile or compressive axial load.

TABLE OF CONTENTS

ILLUSTRATIONS

SYMBOLS

A,B,C,D,E,F,G	Corners of maximum shear stress yield surface
A',B',C',D',E',F',G'	Corners of maximum reduced stress yield surface
$H = \sum dQ_i dq_i^p / \sum dq_i^p dq_i^p$	Strain hardening rate
N	Excess axial force on tube with closed ends
P	Pressure
$Q = \pi b^2 P$	Pressure parameter
Q_i	Generalized stresses
T	Total axial force on tube with open ends
U	Energy dissipation rate
a	Internal radius of tube
b	External radius of tube
e	Base of natural logarithms
$f = N/\pi b^2 \sigma_o$	Excess axial force parameter
$p = P/\sigma_o$	Pressure parameter
q_i^p	Generalized plastic strains
r,θ,z	Cylindrical coordinates
r', r_1	Radii of stress discontinuities
u,v,w	Velocities
$\beta = b/a$	Thickness ratio

$\overline{\gamma}_{r\theta} = \epsilon_r - \epsilon_\theta$, etc.	Maximum shear strains
$\overline{\epsilon} = ((\epsilon_r-\epsilon_\theta)^2+(\epsilon_\theta-\epsilon_z)^2+(\epsilon_z-\epsilon_r)^2)^{1/2}/\sqrt{3}$	Effective strain
$\epsilon_r, \epsilon_\theta, \epsilon_z$	Principal strain rates (in Part I): principal strains (in Part II)
$\epsilon_q = 2\epsilon_\theta\Big]_{r=b} + \epsilon_z$	Generalized strain rate corresponding to Q
$\lambda = \epsilon_\theta/\epsilon_z$ at $r = a$	
μ, ν	Positive numerical coefficients
$\sigma = (\sigma_r+\sigma_\theta+\sigma_z)/3$	Mean stress
σ_o	Yield stress in simple tension
$\sigma_r, \sigma_\theta, \sigma_z$	Principal stresses
$t = T/\pi(b^2-a^2)\sigma_o$	Axial force parameter

PART I

ANALYSIS OF COMPLEX STRESS STATES IN THE TUBE TEST

R. M. Haythornthwaite

1. INTRODUCTION

During plastic deformation, it is quite possible that stress states frequently occur which are complex, in the sense that they are not reducible to states of either simple shear or simple tension merely by subtracting a hydrostatic pressure component. Important exceptions are plane strain, in which the stress states are reducible to simple shear, and certain cases of axial symmetry where the stresses are reducible to simple tension. In these cases analysis can proceed on the basis of a knowledge of a single yield strength. In general, however, no restriction can be placed on the nature of the stress state and analysis must be based on the premise that each and every complex stress state could occur somewhere in the yielding body.

This circumstance places a substantial premium on a detailed knowledge of the yield criterion of the material. If, for example, only a single yield strength is known, the yield surface can vary widely in shape even when there is good reason to believe the material can be treated as an isotropic, ideally plastic body.[1] The situation for the particular case where the yield criterion is insensitive to the hydrostatic component of stress is indicated in Fig. 1, which shows crosssections formed by the intersection of an octahedral plane ($\sigma_1+\sigma_2+\sigma_3$ = const.) with yield surfaces drawn in the space of principal stresses. The requirements of symmetry and convexity for the isotropic, ideally plastic material dictate the largest and smallest yield surfaces which can be drawn through a known value of the yield strength in simple tension (Fig. 1a) or through a known value of the yield strength in simple shear (Fig. 1b). In the absence of further information, it is then necessary to use the inner yield surface to determine lower bounds and the outer surface to determine upper bounds. There must remain a substantial element of uncertainty as to the actual yield load of any structure, amounting to as much as ±7% in some cases,[1] an uncertainty that can be narrowed only by first obtaining further information on the yield strength of the material under complex stress states.

Observations of the yield point for complex stress states are not straightforward because it seems impossible to find a practical test in which the stress distribution is statically determinate and hence independent of the yield and flow properties of the material. A common approach has been to assume quite arbitrarily that the stresses are uniform when one dimension is made sufficiently small and often the elastic stress distribution has been quoted to justify this step. A plastic material may behave in a highly discontinuous manner, however, and the procedure has introduced an element of uncertainty in the interpretation of test results.

An alternative and perhaps overlooked approach would be to seek a test situation where the displacements of the body are kinematically determinate in the

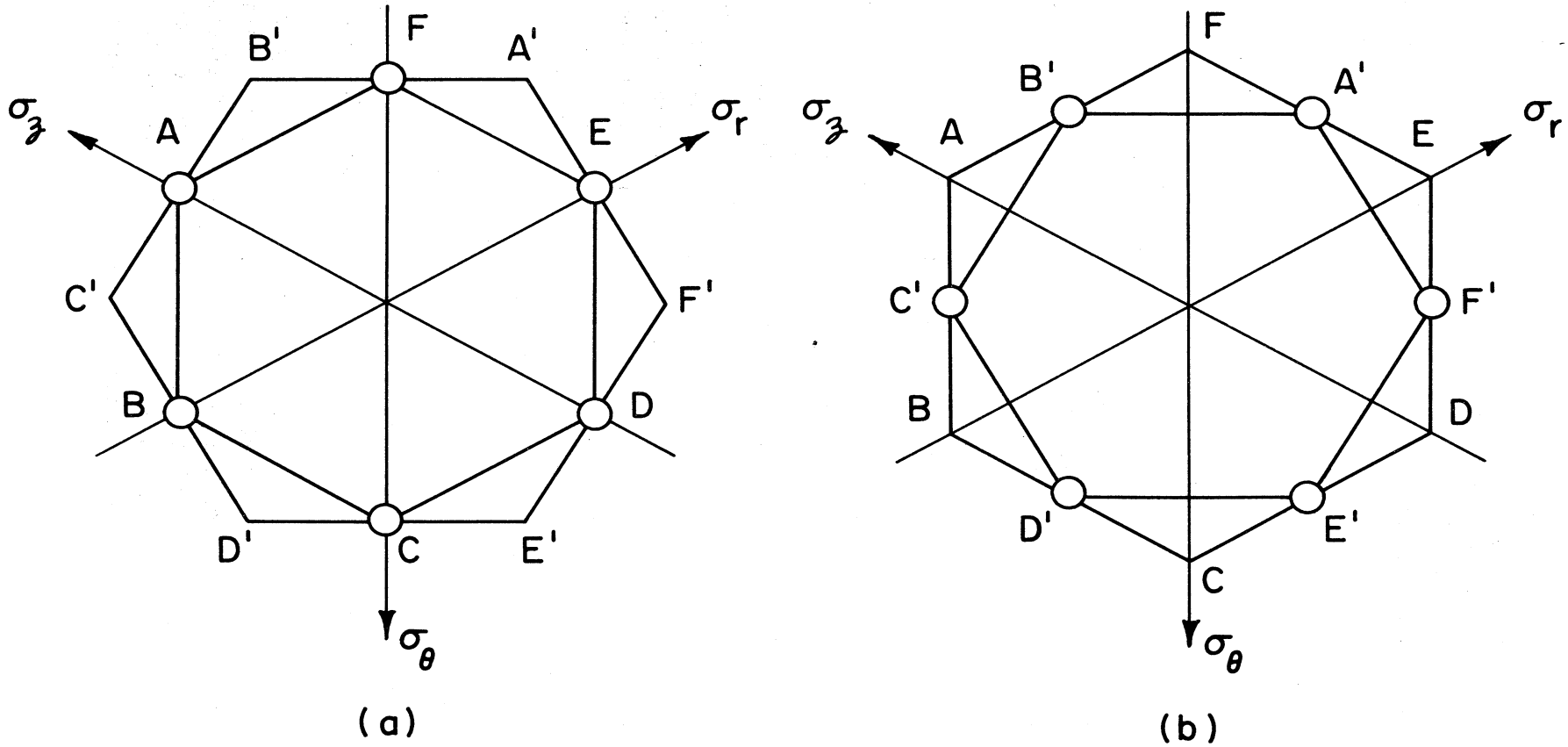

Fig. 1. Bounding yield criteria in accordance with the theory of ideally plastic, isotropic bodies (a) when the yield strength of the material is known in simple tension and (b) when the yield strength is known in simple shear. ABCDEF represents the maximum shear stress criterion:

$$\text{max. } \{|\sigma_r-\sigma_\theta|,\ |\sigma_\theta-\sigma_z|,\ |\sigma_z-\sigma_r|\} = \sigma_o$$

and A'B'C'D'E'F' the maximum reduced stress criterion

$$\text{max. } \{|\sigma_r-\sigma|,\ |\sigma_\theta-\sigma|,\ |\sigma_z-\sigma|\} = \frac{2}{3}\sigma_o\ .$$

sense that they can be evaluated in terms of boundary motions without reference to the stress distribution. In the case of material in which the yield strength is independent of the hydrostatic component of stress, the stress distribution is then known except for the hydrostatic component and that, hopefully, can be found from equilibrium requirements. Such kinematic determinacy obviously requires a high degree of symmetry, and it turns out that the long tube is an example. It is possible to make a complete analysis of the initial motion problem for the ideal rigid-plastic material, and to compare performance for various yield criterias including, most significantly, the bounding criteria that appear in Fig. 1.

A fact emerges which is at first sight surprising: not only does the stress distribution vary widely according to which yield criterion is supposed to apply, but also the stress distribution across the thickness may be highly nonuniform and this nonuniformity persists even when the tube is indefinitely thin. When extremum yield criteria are employed, average stress becomes almost meaningless at some load ratios, so the appropriateness of the uniform stress assumption depends on the nature of the yield criterion.

The tube subject to various combinations of lateral pressure and axial force has been studied intensively,[2-25] but the majority of studies have been restricted, at least so far as detailed investigations are concerned, to three special cases: open tubes, closed tubes, and tubes which are axially constrained. Important exceptions are the complete solution in parametric form obtained recently by Panarelli and Hodge using the v. Mises' yield criterion[25] and the general discussion of solutions associated with various facets of the Tresca (maximum shear stress) criterion by Kammash, Murch, and Naghdi.[23] The Tresca criterion was also employed in significant earlier studies by Koiter[18] and Bland.[19] The development given below owes much to the work of these authors. In order to keep the presentation uncluttered, attention will be confined to a rigid, ideally plastic material in which yield is independent of the level of mean stress. Such a material remains rigid until a yield stress is reached and is then capable of deforming indefinitely according to the flow law associated with materials that must always absorb work in any loading cycle.[26,27] One important consequence of assuming yield is independent of the mean stress for such a material is that no volume change occurs during the subsequent plastic flow. The deformations of all elements of the tube are then obtained easily in terms of the surface displacement.

The analysis defines the form of the yield surface, drawn in the space of the applied tractions, which is associated with each of the extremum criteria shown in Fig. 1. The choice of yield criterion makes a substantial difference to the shape of the yield surface in traction space; hence comparison of various observed tractions (which may be plotted directly in the space) can lead to rational selection of the yield criterion most appropriate for any particular material.

2. TUBES UNDER AXIAL LOAD AND INTERNAL PRESSURE

We shall consider the initial motion of a long, right circular tube, internal radius a and external radius b, when subject to an internal pressure P and an axial force T. Cylindrical coordinates r, θ, z, as shown in Fig. 2,

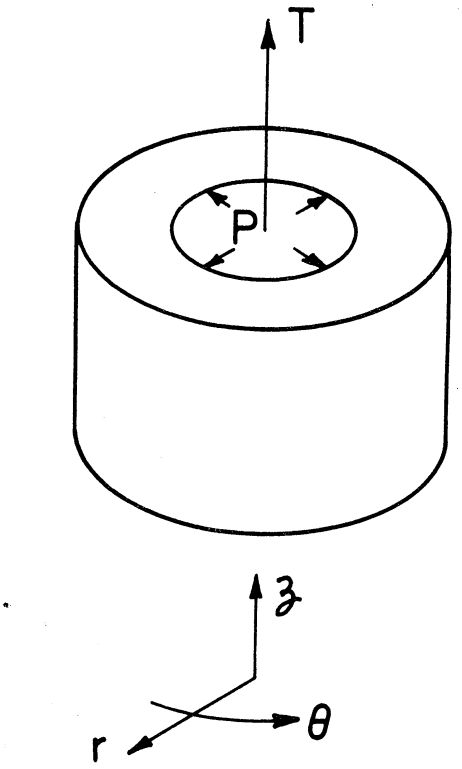

Fig. 2. Notation for tube analysis.

will be used. This case is entirely equivalent to the general one of differential internal and external pressure in the case where the yield strength of the material is unaffected by the addition of hydrostatic pressure component, as will be assumed here. It is convenient to introduce the nondimensional load parameters

$$p = \frac{P}{\sigma_o}$$
$$t = \frac{T}{\pi(b^2-a^2)\sigma_o} \qquad (1)$$

where σ_o is the yield strength of the material in simple tension.

By symmetry there will be no circumferential velocity, and the other velocity components will be independent of θ, so solutions will be sought based on the velocity field

$$\left.\begin{aligned} u &= u(r) \\ v &= 0 \\ w &= \epsilon_z z \end{aligned}\right\} \qquad (2)$$

where the axial strain rate ϵ_z is the same at all points in the tube. The field (2) does not admit bulging; however the associated stress distributions may well be valid for other velocity fields in which a finite length of the tube deforms, the rest remaining rigid. Shield[28] has found this to be so for the special case of the tension/compression test. Substituting Eq. (2) in the expression for zero volume change:

$$\epsilon_r + \epsilon_\theta + \epsilon_z = \frac{\partial u}{\partial r} + \frac{u}{r} + \frac{\partial w}{\partial z} = 0 \qquad (3)$$

and integrating, we obtain

$$\epsilon_r : \epsilon_\theta : \epsilon_z = -\left(\lambda + \frac{1}{2}\right)\frac{a^2}{r^2} - \frac{1}{2} : \left(\lambda + \frac{1}{2}\right)\frac{a^2}{r^2} - \frac{1}{2} : 1 \qquad (4)$$

where λ is the ratio between ϵ_z and ϵ_θ at $r = a$:

$$\epsilon_\theta\Big]_{r=a} = \frac{u}{r}\Big]_{r=a} = \lambda\epsilon_z \qquad (5)$$

The ratio of principal strains is known everywhere in terms of λ, so the rate of energy dissipation associated with a given yield criterion can be computed. Equating the internal and external work done would then lead to a relationship between the external tractions in terms of the parameter λ. This is formally an upper bound because the body is not necessarily in equilibrium.

A slightly less direct procedure will be adopted which has the advantage that a complete solution is obtained, not just an upper bound. Stresses are associated with the principal strain rate ratios and then the tractions are found by using equilibrium. The resulting stress distribution is statically admissible and at the same time compatible with an admissible velocity field; hence it is the actual solution. A further advantage of this approach is that the relation between the tractions is found explicitly instead of in parametric form.

Attention will be concentrated on the extremum yield criteria discussed in the Introduction because these criteria result in the largest possible variations in the applied tractions which can be accommodated within the framework of ideal plasticity theory. Both these yield surfaces are made up from segments of six intersecting planes. The stresses associated with a given strain rate ratio, as expressed in Eq. (4), can be found in part by noting that the strain rate vector associated with a given point on the yield surface is directed along the outwards drawn normal of a plane which is a supporting plane to the yield surface at the stress state point.[29] All strain rate vectors lie in the octahedral plane $\epsilon_r+\epsilon_\theta+\epsilon_z = 0$, thus evidencing constancy of volume during plastic flow, and equally the direction of the stain rate vector cannot be used to dis-

tinguish between stress states related by the addition or subtraction of a hydrostatic pressure component ($\delta\sigma_r = \delta\sigma_\theta = \delta\sigma_z$). In boundary value problems where traction boundary conditions predominate, the stress distribution is often completely or almost completely determinate from equilibrium despite the presence of multiple flats on the yield surface, and this proves to be so in the case of the tube.

MAXIMUM SHEAR STRESS YIELD CRITERION

This criterion is represented by the inscribed polygon ABCDEF in Fig. 1a. The stress state associated with a certain ratio of principal strain rates can be identified in the manner described below. The stress state point will be at A when $\epsilon_z > 0$ and $|\epsilon_z| > |\epsilon_r|$, $|\epsilon_\theta|$, and at B when $\epsilon_r < 0$ and $|\epsilon_r| > |\epsilon_z|$, $|\epsilon_\theta|$, etc., so the appropriate corner is determined by the identity of the principal strain which has the largest value, together with the sign of that strain. The stress state point may be somewhere on a side only when one strain rate is zero, e.g., on AB (including the end points), only when $\epsilon_\theta = 0$ and $\epsilon_z > 0$.

The stress states associated with various values of λ and r can now be identified. By inspection of Eq. (4), it is easily verified that state point B (requiring $|\epsilon_r| > |\epsilon_z|, |\epsilon_\theta|$) will be reached when

$$\left(\frac{r}{a}\right)^2 < 2\lambda + 1 \qquad (6)$$

and from this and similar results a phase diagram, Fig. 3, can be constructed. The three stress states shown are those appropriate for the case $\epsilon_z > 0$.

The phase diagram reveals a surprisingly complex stress pattern. For any instant a horizontal line in Fig. 3 will trace the stress states at various radii. If, for example, $\lambda > 0$, there will always be an inner zone at state point B and an outer zone at state point A, however thin the tube. Likewise if $\lambda < -1$, there will always be an inner zone at state point F and an outer zone at state point A. The discontinuities between state points B and A and between state points F and A are different in nature, as is clear from examination of the Mohr circles in Fig. 3. The former represents a discontinuity in σ_θ only, while the latter represents a discontinuity in both σ_θ and σ_z, σ_r remaining constant across the discontinuity, for equilibrium.

The transitions from B to A and from F to A occur when ϵ_θ and ϵ_r are zero, respectively, and so state points on the sides AB and AF, Fig. 1a might be present; however the transitions occur at particular radii, so ambiguity in the stress state is restricted to these radii and equilibrium is unaffected. On the other hand, when ϵ_z is zero, as will be the case when λ becomes indefinitely large (or small), state points on BC and on FE, Fig. 1a can be present. This case will be examined first.

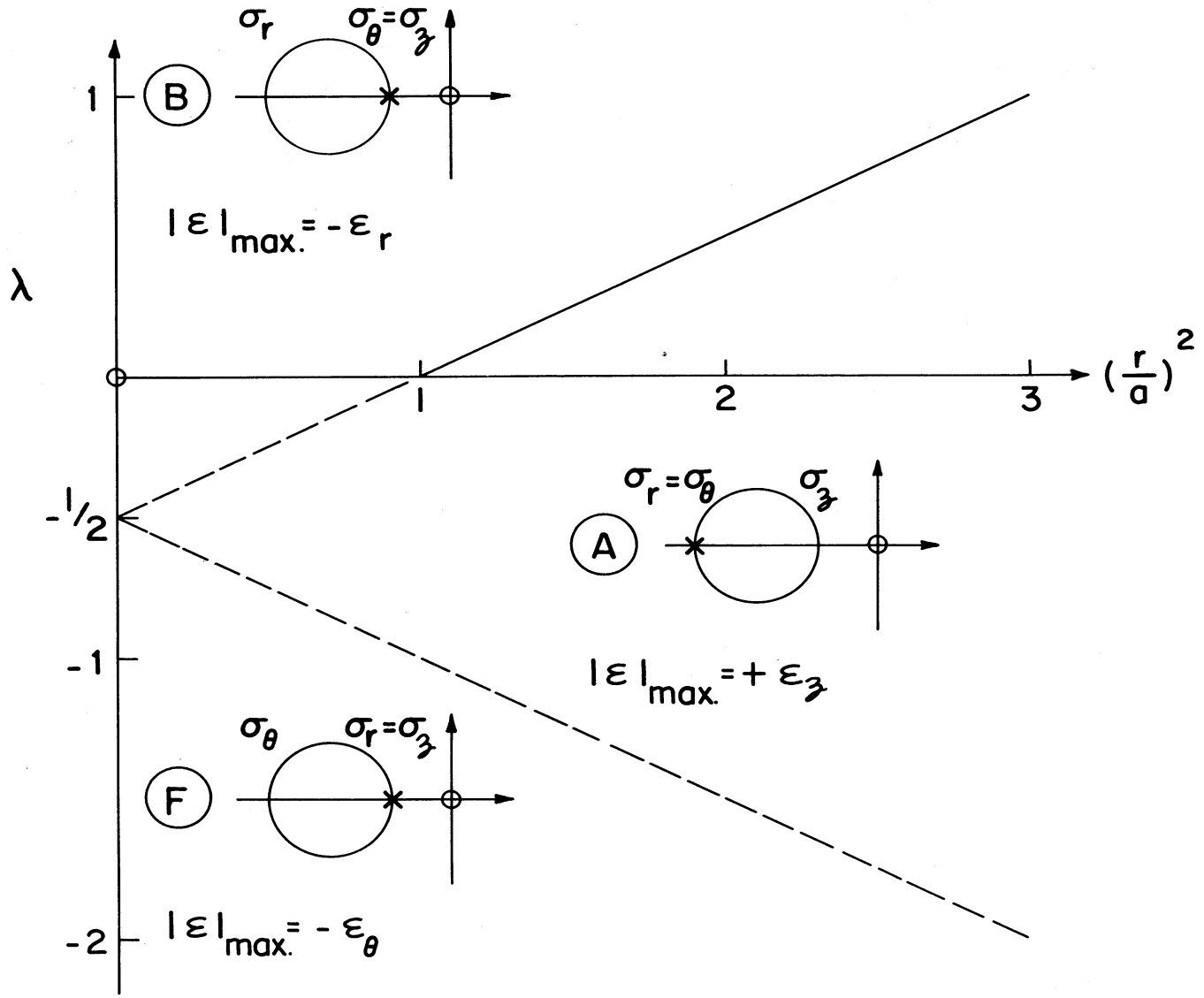

Fig. 3. Maximum shear stress criterion of yield for material of a tube: phase diagram for stress states at various radii in terms of the coefficient λ.

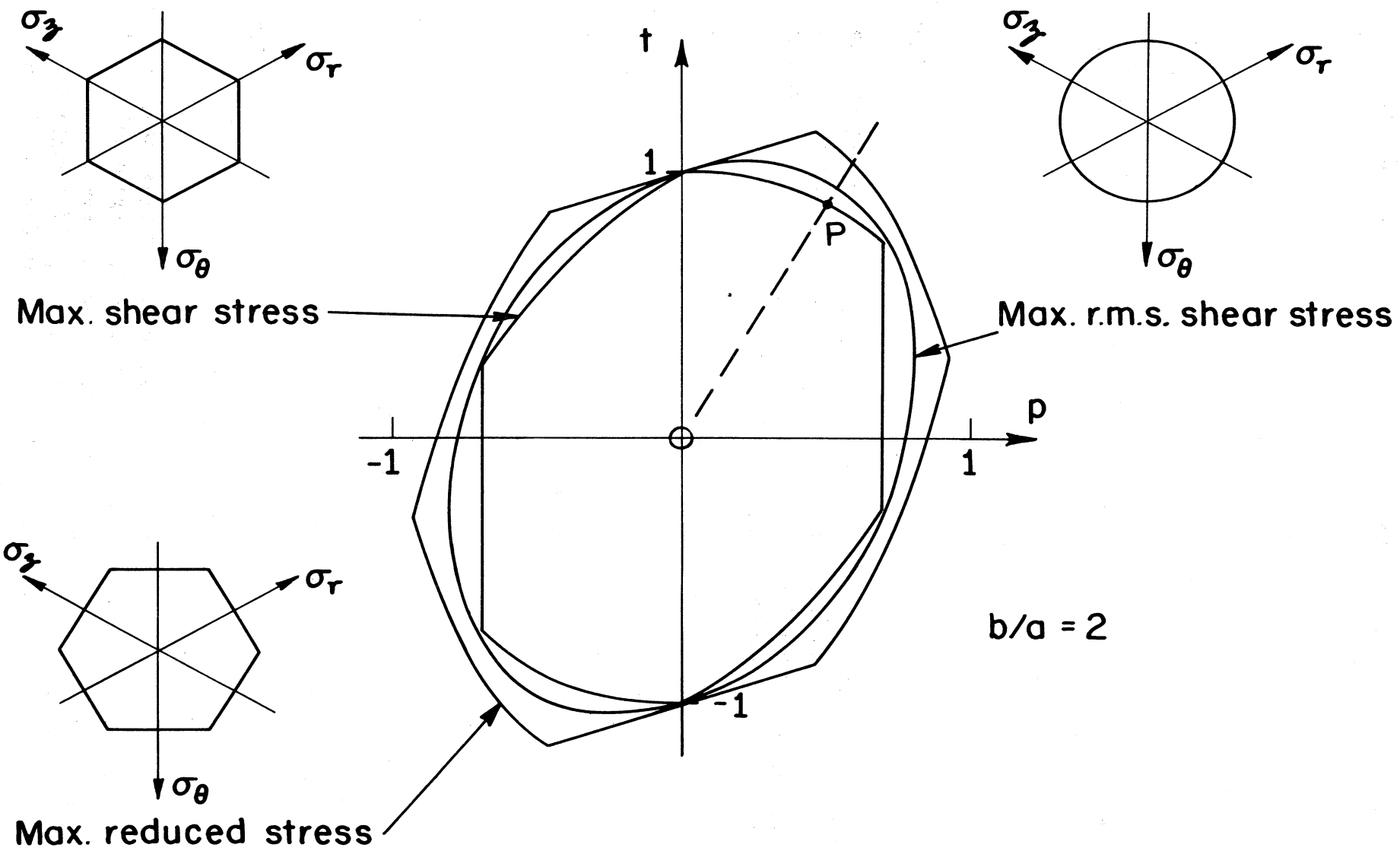

Fig. 4. Tube under combined axial load and internal pressure; $\beta = 2$. Yield curves, in the traction plane, corresponding to three yield criteria for the material.

On BC, Fig. 1a, the intermediate principal stress is σ_z, so by the maximum shear stress yield criterion,

$$\sigma_\theta - \sigma_r = \sigma_o \tag{7}$$

For radial equilibrium

$$\frac{d\sigma_r}{dr} + \frac{\sigma_r - \sigma_\theta}{r} = 0 \tag{8}$$

Substituting Eq. (7) in Eq. (8), integrating and making use of the boundary condition

$$\sigma_r \Big]_{r = b} = 0 , \tag{9}$$

we obtain

$$\sigma_r = \sigma_o \ln(r/b) \tag{10}$$

The only restriction is that σ_z should remain the intermediate principal stress. Limiting cases are $\sigma_z = \sigma_\theta$ (point B) and $\sigma_z = \sigma_r$ (point C). The corresponding values of t, found by evaluating σ_z from Eqs. (7) and (9), followed by integration over the radial cross-section of the tube, are

$$t = \ln\beta/(\beta^2-1) \pm \frac{1}{2} \tag{11}$$

where $\beta = b/a$. Finally, on substituting the boundary value

$$\sigma_r \Big]_{r = a} = P \tag{12}$$

in Eq. (9),

$$\begin{gathered} p = \ln\beta \\ \frac{\ln\beta}{\beta^2-1} + \frac{1}{2} \geq t \geq \frac{\ln\beta}{\beta^2-1} - \frac{1}{2} \end{gathered} \tag{13}$$

and by a parallel computation for side EF:

$$\begin{gathered} p = -\ln\beta \\ -\frac{\ln\beta}{\beta^2-1} + \frac{1}{2} \geq t \geq -\frac{\ln\beta}{\beta^2-1} - \frac{1}{2} \end{gathered} \tag{14}$$

The stress σ_z remains indeterminate. Possible distributions include uniform stress across the entire thickness, in which case the stress point would be somewhere on a side of the yield surface, or a discontinuous distribution in which the stresses are represented by one corner of the yield surface for an outer layer and by another corner for an inner layer. Despite this indeterminacy

of the stresses, the yield surface in traction space remains unique (see Appendix I of Ref. 30).

When $\lambda>0$, $\epsilon_z>0$, the phase diagram, Fig. 3, indicates there will be an inner zone at state point B and an outer zone at state point A, Fig. 1a. The radius r' of the interface is found to be

$$r' = ae^p \tag{15}$$

by integrating Eq. (8) for both zones, after noting that in the inner zone $\sigma_\theta = \sigma_r$ and in the outer zone $\sigma\theta = \sigma_z$. In the outer zone, $\sigma_z = \sigma_o$ and in the inner zone

$$\sigma_z = \sigma_o(\ln(r/a)-p+1) \tag{16}$$

and by integration over the cross-section

$$(\beta^2-1)t = p + \beta^2 - \frac{1}{2}(1+e^{2p}) \tag{17}$$

Similar integrations can be carried out for the case $\lambda<0$, $\epsilon_z>0$ and for the two cases where $\epsilon_z<0$, the results being summarized by

$$(\beta^2-1)t = p \pm \left(\beta^2 - \frac{1}{2}(1+e^{2|p|})\right) \tag{18}$$

The complete yield criterion in the p-t plane is shown as the inner closed curve in Fig. 4.

MAXIMUM REDUCED STRESS YIELD CRITERION

This criterion is represented by the circumscribed polygon A'B'C'D'E'F' in Fig. 1a. In identifying the stress states associated with the various sides and corners of this surface, it is convenient to introduce the notations $\bar{\gamma}_{r\theta} = \epsilon_r-\epsilon_\theta$, etc., to denote the maximum shear strain rate. The strain rates associated with side A'B', Fig. 1a, are $\epsilon_r:\epsilon_\theta:\epsilon_z = 1/2:-1:1/2$, so that $\bar{\gamma}_{r\theta}:\bar{\gamma}_{\theta z}:\bar{\gamma}_{zr} = 1:-1:0$ and those associated with A'F' are $\epsilon_r:\epsilon_\theta:\epsilon_z = 1:-1/2:-1/2$, so that $\bar{\gamma}_{r\theta}:\bar{\gamma}_{\theta z}:\bar{\gamma}_{zr} = 1:0:-1$. Thus the strain rate ratios associated with corner A' will be $\bar{\gamma}_{r\theta}:\bar{\gamma}_{\theta z}:\bar{\gamma}_{zr} = \mu+\nu:\mu:-\nu$ where μ,ν are positive numbers. Hence the stress point will lie at A', Fig. 1a, when $\bar{\gamma}_{r\theta}>0$ and $|\bar{\gamma}_{r\theta}|>|\bar{\gamma}_{\theta z}|, |\bar{\gamma}_{zr}|$. Similar criteria can be obtained for the other corners, so the appropriate corner is determined by the identity of the shear strain rate $\bar{\gamma}$ which has the largest value, together with the sign of that strain. The stress point will be on a side only when one of the maximum shear strains is zero, i.e., when two principal strains are equal.

Equation (4) can be rewritten in terms of the maximum shear strain rates:

$$\bar{\gamma}_{r\theta} : \bar{\gamma}_{\theta z} : \bar{\gamma}_{zr} = -2\left(\lambda+\frac{1}{2}\right)\frac{a^2}{r^2} : \left(\lambda+\frac{1}{2}\right)\frac{a^2}{r^2} - \frac{3}{2} : \left(\lambda+\frac{1}{2}\right)\frac{a^2}{r^2} + \frac{3}{2} \tag{19}$$

so state point A' will be reached when

$$\left(\frac{r}{a}\right)^2 < -\frac{2\lambda+1}{3} \tag{20}$$

State point B' will apply for larger values of λ below $\lambda = -1/2$, then state point C' will apply, to be superceded by state point D' when

$$\left(\frac{r}{a}\right)^2 > \frac{2\lambda+1}{3} \tag{21}$$

The phase diagram constructed from these results is shown in Fig. 5. The stress states referred to above, which are appropriate for $\epsilon_z > 0$, are shown in the inserts.

As in the case of the maximum shear stress criterion, it is again evident that, for certain ranges of λ, there will be two stress zones, with a stress discontinuity between them. The transitions from A' to B' and from C' to D' occur when $\overline{\gamma}_{zr}$ and $\overline{\gamma}_{\theta z}$ are zero, respectively, but the latter happens only at isolated radii, according to Eq. (19), and not over a finite band, so there are evidently stress discontinuities at these radii. On the other hand, Eq. (19) indicates that the transition from B' to C', Fig. 1a, which occurs when $\overline{\gamma}_{r\theta}$ is zero, can occur simultaneously at all radii. Unless eliminated by a consideration of equilibrium, alternative stress distributions may be possible. This latter case will be dealt with first.

Suppose an inner zone at stress state B', Fig. 1a, and an outer zone at stress state C', and denote the radius at which the stress discontinuity occurs by r_1. For the inner zone $\sigma_r - \sigma_\theta = 2/3\ \sigma_o$ and for the outer zone $\sigma_r - \sigma_\theta = -2/3\ \sigma_o$, so substituting each of these equations in turn in the equation of equilibrium, Eq. (8), integrating, and substituting the boundary conditions, Eqs. (9) and (12), we obtain

$$\sigma_r = P - \frac{2}{3}\sigma_o \ln\left(\frac{r}{a}\right) \tag{22}$$

for the inner zone and

$$\sigma_r = \frac{2}{3}\sigma_o \ln\left(\frac{r}{b}\right) \tag{23}$$

for the outer zone.

The position of the interface is determined by equating values of σ_r across it, hence

$$r_1 = (ab)^{1/2} e^{3p/4} \tag{24}$$

The axial stress σ_z is equal to $\sigma_r + 2\sigma_o/3$ in the inner zone and $\sigma_r + 4\sigma_o/3$ in the outer zone and the total axial force is found by integration: the resulting relationship between p and t is

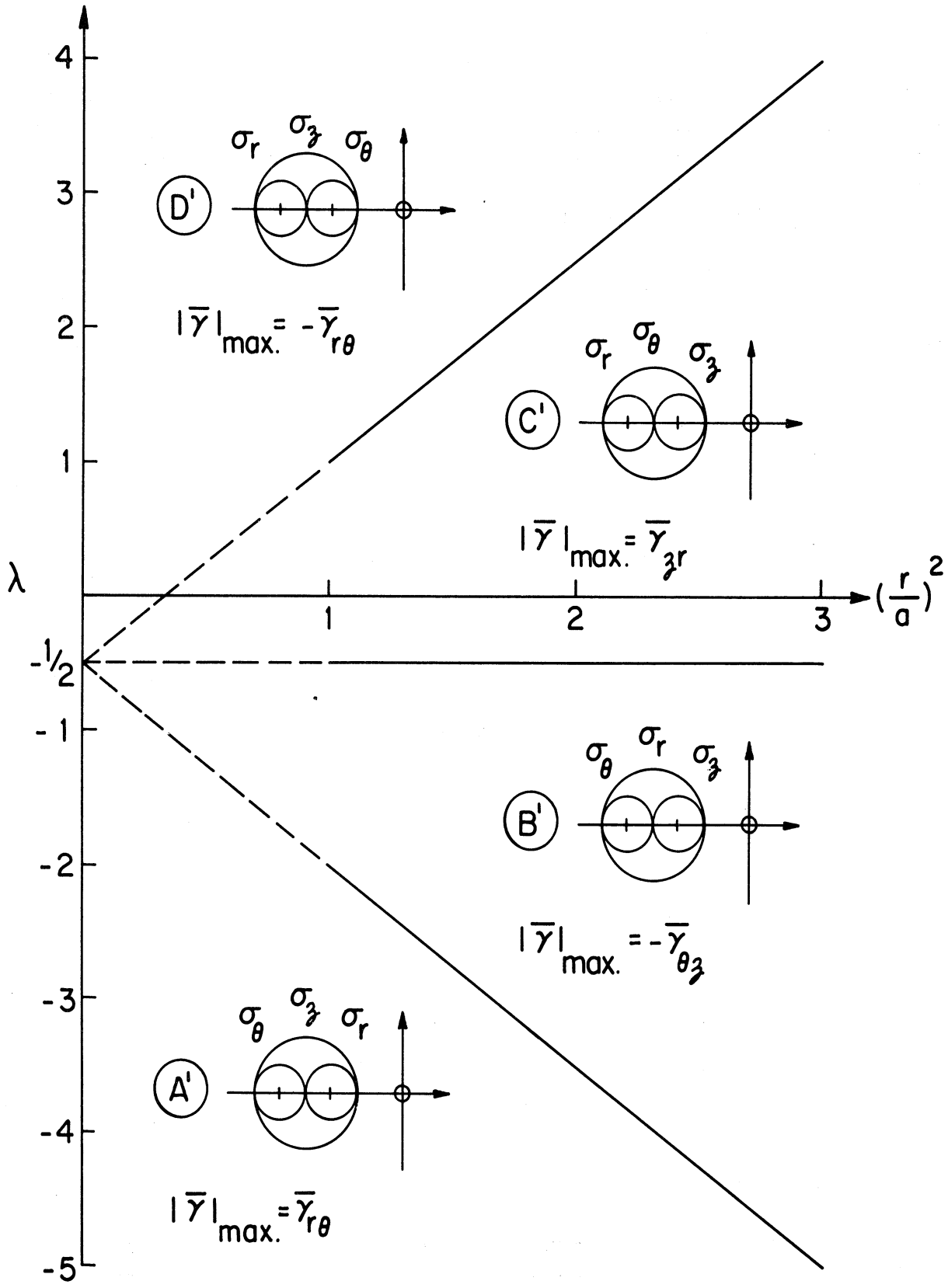

Fig. 5. Maximum reduced stress criterion of yield for material of a tube: phase diagram for stress states at various radii in terms of the coefficient λ.

$$p = (\beta^2-1)(1-t) \tag{25}$$

The stress distribution used above serves to show that an equilibrated set of stresses can be found; however, it is not unique. It can be readily shown that the stress distribution associated with σ_z = const. can also be equilibrated. Of course, this and the many other possible alternatives give rise to the same relation, Eq. (25) between p and t.

When $\lambda>1$ and $\epsilon_z>0$, Fig. 5 indicates there will be an inner zone at state point D' and an outer zone at state point C'. A procedure parallel to that described above is applied and it is found that the interface is at a radius

$$r_1 = a^2b^{-1}e^{3p/2} \tag{26}$$

and the formula relating p and t is

$$(\beta^2-1)t = p + (\beta^2-\beta^{-2}e^{3p})$$

Similar integration can be carried out for the case $\lambda<-2$, $\epsilon_z>0$ and for the two cases where $\epsilon_z<0$, the results being summarized by

$$(\beta^2-1)t = p \pm (\beta^2-\beta^{-2}e^{3|p|}) \tag{27}$$

The yield criterion in the p-t plane is shown as the outer closed curve in Fig. 4.

MAXIMUM R.M.S. SHEAR STRESS YIELD CRITERION

In this criterion, which is frequently associated with the names of Huber and v. Mises, yield occurs when stresses on the surface

$$(\sigma_r-\sigma_\theta)^2 + (\sigma_\theta-\sigma_z)^2 + (\sigma_z-\sigma_r)^2 = 2\sigma_o^2 \tag{28}$$

are reached. The corresponding cross-section in Fig. 1 is a circle centered at the origin. Adoption of this criterion often leads to greater analytical difficulties but, in the case of most poly-crystalline metals, it has the merit that it provides a closer approximation to the actual behavior than either of the extremum criteria shown in Fig. 1.

An analysis based on this criterion has been given by Panarelli and Hodge,[25] who obtain a relation between p and t in parametric form; however, a solution in closed form results if the procedures that have been used in the case of the extremum criteria are followed once more. The solution is

$$(\beta^2-1)t = p \pm (1+\beta^4+2\beta^2(1-X^2)^{-1/2})^{1/2} \tag{29}$$

where $X = (1-e^{2\sqrt{3}|p|})/(1+e^{2\sqrt{3}|p|})$. The corresponding yield line has been added to Fig. 4.

In the above analysis, the yield stress in simple tension, σ_o, has been incorporated in the definition of the nondimensional load parameters p, t, Eq. (1). In consequence the three yield criteria plotted in Fig. 4 coincide at the point t = 1, p = 0, which corresponds to simple axial tension and the point t = -1, p = 0 which corresponds to simple axial compression. Thus the yield curves in Fig. 4 are in the relative position which would obtain when the yield surfaces in principal stress space are as shown in Fig. 1a. If instead the scale were standardized on the basis that the yield stress in simple shear were known, as in Fig. 1b, then the yield curves in the traction plane would coincide on the line

$$(\beta^2-1)t = p \qquad (30)$$

The high degree of nonuniformity of the stress distributions can be best appreciated by considering a specific case. Figure 6 shows the stress distribu-

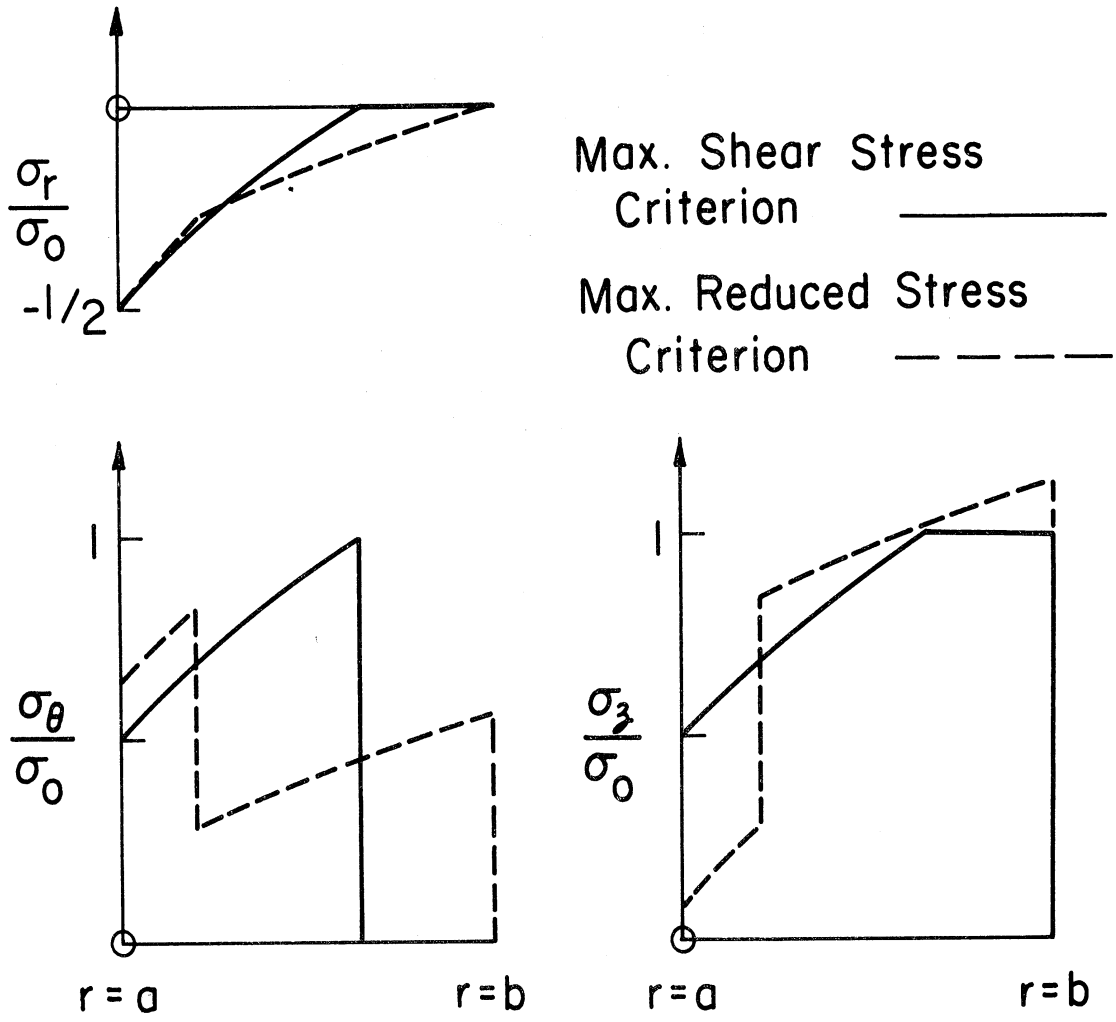

Fig. 6. Tube under combined axial load and internal pressure; $\beta = 2$. Stress distributions for the load path shown as the dotted line in Fig. 4.

tions associated with the extremal yield criteria for the case $\beta = 2$ when the stress state points lie on the dotted line shown in Fig. 4. Bearing in mind that the relative scales of the alternative yield criteria can be adjusted, and, in Fig. 4, a common value σ_o of the yield stress in simple tension has been taken just for convenience, both the stress distributions have been drawn for the external tractions associated with point P in Fig. 4. The distribution of σ_r, Fig. 6, is similar for the two extremal criteria, but by no means identical, while the distributions for σ_θ and σ_z differ markedly. In the case of both criteria, the stress discontinuities occur at the radii where the stress state point jumps from one corner to another in Fig. 1. For the maximum shear stress criterion the jump is from corner A in the outer zone to corner B in the inner zone, while for the maximum reduced stress criterion the jump is from corner C' to corner D'.

The above analysis has been described in detail to document the fact that the stress distribution is highly dependent on the form of the yield criterion. Average stresses may be almost meaningless even for a very thin tube. If one of the extremal yield criteria apply, it is possible that many combined stress states cannot be reached whatever external tractions are imposed. For example, if the maximum shear stress criterion holds, then during deformation the intermediate principal stress might always coincide with the largest or the smallest principal stress, although this is not known for certain because the stress distribution is not always unique. It is not known whether either of the extremal criteria will hold for an actual material which may be of interest; however the analysis makes it clear that in the absence of specific further information there is no guarantee a complete range of complex stress states can be induced in the tube test. In any case the simple assumption that the stress is homogeneous may lead to substantial errors in the interpretation of test results. This point is discussed in some detail in the next section.

3. THE INTERPRETATION OF EXPERIMENTAL DATA

The above analysis has shown how large the nonuniformities in stress distribution can be in the tube test and hence how misleading it is to interpret this test by the use of mean stresses. It becomes necessary to plot tractions rather than stresses, and to adopt the somewhat indirect procedure of determining curves in the plane of applied tractions which are associated with the various yield criteria. Generally speaking, the test data will not coincide exactly with one or other of these theoretical curves and the precise yield criterion being followed by the material then becomes a matter for speculation. This may not be important in practice, however, because a precise representation of the yield criterion is of limited use as a starting point in analysis, due to mathematical difficulties. It is of much greater concern to employ a method of interpretation of the data itself which, because it does not introduce approximations of uncertain accuracy, permits selection of the mathematically simple yield criterion which provides the closest fit to the data.

What are the errors in interpretation introduced by assuming the stress distribution is uniform in the case of a tube of practical dimensions which allow the maintenance of reasonable tolerances on the thickness variation? A comparison for some steel tubes tested recently at The University of Michigan is shown in Fig. 7. It is seen that the errors can amount to 5% or more, which

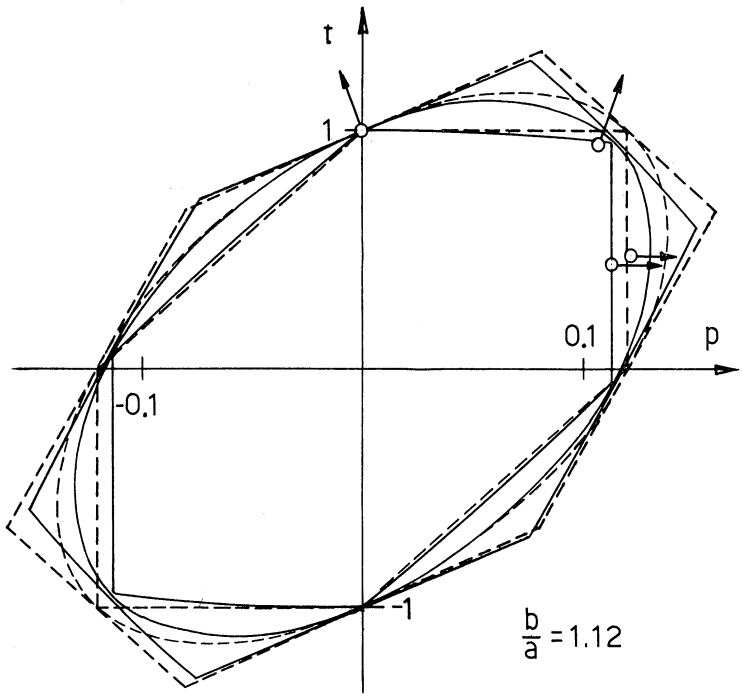

Fig. 7. Tube under combined axial load and internal pressure; $\beta = 1.12$. Comparison of test data (circles) for steel tubes with the theory for ideally plastic bodies (full lines) and theory based on assuming uniform stress (dotted lines).

could be significant when a choice is being made between the yield criterion to provide the closest fit to test data.

Figure 7 illustrates the interesting fact that the extremal criteria virtually coincide at four points in addition to the two points where they are made to coincide by the adjustment of scales. The curves are near enough together to provide an accurate check on the isotropy of the material which is not dependent on any assumption about the nature of the yield criterion. On the other hand, use of the approximate curves (shown dotted in Fig. 7) might well lead to the conclusion that anisotropy of yield strength is present when this is not the case.

The above interpretations and analysis are valid only if the material can be approximated by an isotropic, ideally plastic material model of the type used in classical plasticity theory. There is of course no guarantee that any one material will fall into this category, however, evidence is accumulating that it is a useful and reasonably accurate model for many metals. In the case of the small amount of test data added to Fig. 7, for example, the arrows indicating the direction of the generalized strain vector corresponding to the tractions p, t lie in directions which are likely to be close to that of the outwards drawn normal to the yield curve, which suggests strongly that the material possesses a stress strain relation of the requisite type. On the other hand considerable caution would have to be exercised in using the above test interpretations for materials such as granular media, for which the appropriateness of an isotropic, ideally plastic model is by no means established.

It is also clear from Fig. 7 that a rational choice of yield criterion can be made on the basis of tube tests. The yield curves associated with the various yield criteria remain well separated in the traction space, Fig. 7, and unless the test data turns out to be very scattered, there should be no difficulty in deciding upon the most appropriate criterion to use in stress analysis.

PART II

EFFECTS OF PRESTRAIN ON PLASTIC FLOW AND FRACTURE IN A STEEL SUBJECT TO COMPLEX STRESS

R. M. Haythornthwaite
D. R. Jenkins
M. D. Coon
C. K. Felber

I. INTRODUCTION

This part will be concerned with the discussion of a program of tests which have been carried out to obtain some provisional information about the effects of prestrain on the flow and fracture properties of a steel subject to complex stress states.

Several previous groups have obtained information on the nature of subsequent yield surfaces in various metals[31-37]; however, for the most part, these investigators did not attempt to get beyond an identification of the presence of subsequent yield, as defined in various ways. Moreover, they invariably interpreted the results in terms of average or surface stresses computed by some more or less arbitrary assumption about the stress distribution. A rereading of Part I of this report is an adequate reminder of the dangers inherent in this approach. Nevertheless, despite the doubts about details of interpretation, these authors have established beyond reasonable question several important points, foremost of which is the striking shift in the position and shape of the yield surface which frequently accompanies plastic deformation.

What has been lacking is an investigation of the affects of plastic deformation on serviceability as it concerns the designer: Can ductility be seriously curtailed by prestraining at other and different stress combinations? What mathematical model is most appropriate for representing a prestrained material (perhaps prestrained due to some unusual overload) for the purposes of a stress analysis? Are certain combinations of prestrain and subsequent strain particularly damaging? In this investigation we cannot do more than suggest tentative answers to these questions and that for a single material, because the effort involved in obtaining minimal experimental information of the right type is so great; however, we hope the work provides a rational framework for further and more detailed studies.

The problem of obtaining reliable information is complicated by the circumstance that the stress distributions may be highly nonuniform even in relatively thin tubes, a point discussed in detail in Part I. As a result, it is necessary to make comparisons between test results and theory in a traction space, rather than in a stress space. Behavior in stress space can only be inferred following relatively sophisticated analysis, analysis which must inevitably rest on premises that may or may not be wholly justified in any particular case.

The study of the data will be based in part on the analysis of Part I, and some results will be restated here in a form convenient for use with the test data. The principal changes are to use as a parameter the axial force N that represents the excess axial force on a closed cylinder, a substitution which has the effect of rendering the yield surface symmetric about the axes, and to

adjust the pressure parameter so that it becomes associated naturally with the outside strain rates, which are those to be observed. The pressure parameter is

$$Q = \pi b^2 P \tag{31}$$

In terms of these parameters, the energy dissipation rate is

$$U = \epsilon_q Q + \epsilon_z N \tag{32}$$

where $\epsilon_q = 2\epsilon_\theta\Big]_{r=b} + \epsilon_z$ and ϵ_z are the "generalized strains" associated with Q and N, respectively.

Introducing the nondimensional parameters

$$\begin{aligned} p &= \frac{P}{\sigma_o} = \frac{Q}{\pi b^2 \sigma_o} \\ f &= \frac{N}{\pi b^2 \sigma_o}, \end{aligned} \tag{33}$$

Eqs. (14) and (18) (for the maximum shear stress criterion) become:

$$p = \begin{cases} \frac{1}{2} \ln(2\beta^2 - 1 - 2\beta^2 |f|) & |f| > \frac{1}{2}(1-\beta^{-2}) \\ \ln\beta & |f| < \frac{1}{2}(1-\beta^{-2}) \end{cases} \tag{34}$$

Equations (25) and (27) (for the maximum reduced stress criterion) become

$$f = \begin{cases} 1 - \beta^{-4} e^{3p} & |p| > \frac{2}{3}\ln\beta \\ 1 - \beta^{-2} & |p| < \frac{2}{3}\ln\beta \end{cases} \tag{35}$$

and Eq. (29) (for the maximum r.m.s. shear stress criterion) becomes

$$f = (1+\beta^{-4}+2\beta^{-2}(1-X^2)^{-1/2})^{1/2} \tag{36}$$

where $X = (1-e^{2\sqrt{3}|p|})/(1+e^{2\sqrt{3}|p|})$.

The rigid-ideally plastic model is the most useful model available for the computation of the ultimate strength of structural components, so it forms a natural backdrop for the assessment of data. Actual materials often exhibit significant strain hardening, and interpretations in terms of a rigid-ideally plastic model are by no means straightforward. The model can, however, be used to represent behavior at various levels of strain hardening provided the data is processed in a suitable fashion.

In the analysis of plastic flow data, it will be assumed, subject to later confirmation, that contours of constant hardening rate (in a space of suitable load parameters) possess properties that make them indistinguishable from yield surfaces of a rigid-ideally plastic solid. These properties[27] are the property of convexity and the property that the vector of (generalized) strains lies in the direction of the outwards drawn normal to the surface, when corresponding (generalized) stresses and (generalized) strains are plotted in the same directions.

The strain hardening rate H will be defined as the magnitude of the component of the generalized stress increment, per unit generalized plastic strain, in the direction of the generalized plastic strain increment, i.e.,

$$H = \frac{\sum dQ_i \, dq_i^p}{\sum dq_i^p dq_i^p} \tag{37}$$

where dQ_i, dq_i^p are increments of generalized stress and strain, respectively. This definition is based on the concept, consonant with plastic theory, that the current yield surface* will remain normal to the generalized strain rate vector, so that the projection of the generalized stress increment dQ_i in the direction of dq_i^p is a measure of hardening (see Fig. 8).

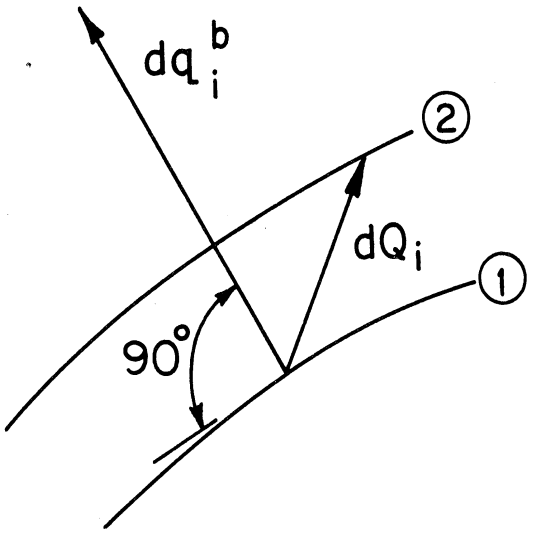

Fig. 8. Local displacement of yield surface during strain hardening.

In terms of the tractions Q, N, with which the strains ϵ_q and ϵ_z as defined in Eq. (32) are associated, the hardening rate will be

*The surface within which only elastic deformation in the neighborhood of the point concerned, occurs.

$$H = \frac{\Delta Q \Delta \epsilon_q + \Delta N \Delta \epsilon_z}{\Delta \epsilon_q{}^2 + \Delta \epsilon_z{}^2} = \frac{\Delta Q(2\Delta \epsilon_\theta + \Delta \epsilon_z) + \Delta N \Delta \epsilon_z}{4\Delta \epsilon_\theta{}^2 + 4\Delta \epsilon_\theta \Delta \epsilon_z + 2\Delta \epsilon_z{}^2} \tag{38}$$

where ϵ_θ is measured on the outside of the tube.

The technique to be adopted in presenting the prefracture plastic flow data will be to plot contours of constant hardening rate. It turns out that the vectors of plastic generalized strain increment are in most cases very nearly normal to these contours, so the contours can be regarded as successive yield surfaces for the purposes of plastic theory.

The basic program of tests comprised series to determine the yield, flow, and fracture properties of the unprestrained material, followed by two series to determine these properties after substantial initial prestraining. In the first series prestraining due to simple tension was used and in the second prestraining due to internal pressure. A comparison of these tests enables some estimates to be made of the influence of prestrain under complex stress on the subsequent flow and fracture properties.

2. TUBE TESTS

The material selected for test was an SAE 1045 cold drawn steel in the form of 1-1/8 in. dia. bar stock. The stock was normalized at 1600°F for 30 minutes, with subsequent air cooling to produce substantially stress relieved material with an initial plastic tensile range prior to strain hardening of about 0.014. Dimensions of the specimens for tests where the excess axial load was to be tensile are shown in Fig. 9. With a view to delaying the onset of buckling, shorter specimens were produced for use when the excess axial load was to be compressive. Each test piece was fitted with three foil strain gages, one mounted circumferentially and the other two axially opposite one another. (These were supplied by W. T. Bean and installed following his directions dated 3/1/64.) These gages were capable of following strains as large as 0.1.

The loading apparatus has been described in an earlier report.[38] In the present series, combinations of internal pressure and axial force were used. It will be recalled that the hydraulic system enables the loads to be increased in a controlled manner while maintaining their ratio at a sensibly constant, preset value. When the specimen was to be tested with an excess axial load which was tensile, the universal joint system described previously[38] was used. This arrangement is intrinsically unstable in compression, however, so for those tests the specimens were mounted on and loaded through hemispherical seatings. The position of a specimen on the seatings was adjusted prior to test to minimize the eccentricity of load, as sensed by the strain gages mounted on it.

Axial load was sensed by a Baldwin SR-4 load cell (capacity 5000, ±5 lb) and the internal pressure in the specimen by a Baldwin SR-4 pressure cell (capacity 20,000, ±20 psi). At moderate strains, the strain gages on the specimen were monitored by hand adjusted Baldwin strain indicators, but when the rate and amount of straining became large, facilities were provided to switch to a Heiland oscillograph recorder, Type 712B which made a continuous autographic trace for later analysis.

Nine specimens were tested to failure without prestraining, eleven were tested following prestrain due to internal pressure (closed ends) and ten following prestrain due to an axial tensile force. Various partial results were obtained from other specimens where the test had to be terminated early. When a prestraining operation was to be performed, this would be done during a morning, followed by adjustment of the machine to a different load ratio and subsequent testing during the afternoon of the same day.

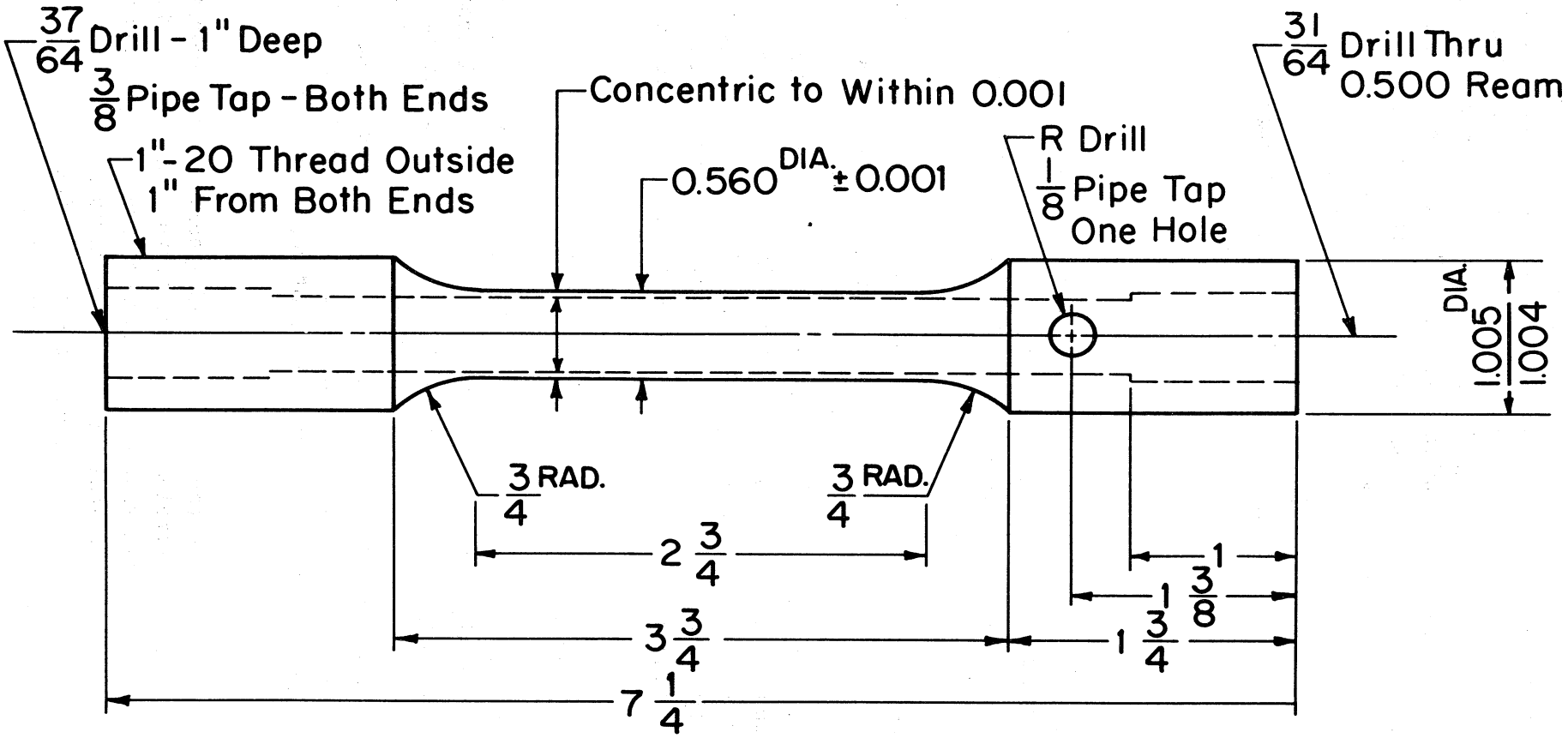

Fig. 9. Dimensions of tubular specimens. The test length was made 1-3/8 in. (instead of the 2-3/4 in. shown) when the excess axial load was to be compressive.

Reduction of the data was accomplished by means of the digital computer. To compensate for the influence of the minor variations in dimensions between specimens, all loads were reduced to equivalent loads (and pressures) on the specimen of nominal dimensions (Fig. 9) on the assumption that the stress distribution was that in the thin elastic cylinder. The latter assumption was necessary because the actual stress distribution could not be known prior to analysis of the data. The error, if any, introduced by this procedure would be of second order compared with the compensations due to variation in dimensions between specimens. For the initial loadings, the corrections were based on the dimensions of the specimens as machined, while for the subsequent loadings the corrections were based on the dimensions after prestrain.

INITIAL YIELD

Loads at which plastic effective strain reached 0.003 on the outsides of the tubes are shown in Fig. 10. A large amount of data is available in the two prestraining directions, and inspection reveals a fairly wide scatter. This is not unusual for initial yield in steels.

For comparison purposes, initial yield curves for the three yield criteria, expressed by Eqs. (34), (35), and (36), have been added to Fig. 10, the scale being fixed so that the curves pass through the mean of the test points for axial tension acting alone ($Q = 0$). Symmetry of the equations enables the comparisons to be made in a single quadrant. The relatively large amount of data available for pure internal pressure ($N = 0$) provides the most significant test of the suitability of the criteria, and it is apparent that, of the three curves shown, the maximum r.m.s. shear stress criterion comes closest to the data.

HARDENING CONTOURS FOR INITIAL AND SUBSEQUENT LOADINGS

Interpretation of continued plastic yielding is based on the definition of the hardening rate H, Eq. (37), which has been discussed in the Introduction to Part II. A digital computer program was employed to compute H using successive observations, and then the tractions for various levels of H were estimated from graphs of H plotted against one or other of the tractions as convenient. By combining data from tests in which various ratios of the tractions were used, it was then possible to construct level curves of constant hardening rate. Examples are shown in Figs. 11 and 12.

Figure 11a shows contours for unprestrained specimens: it records the continuation to larger plastic strains of the same tests as Fig. 10. The initial data again showed considerable scatter and, rather than attempt to pass a curve through the points, the theoretical curve for the maximum r.m.s. shear strain criterion has been superimposed, to a suitable scale (the dotted curves). The outer curve has been sketched through the data points.

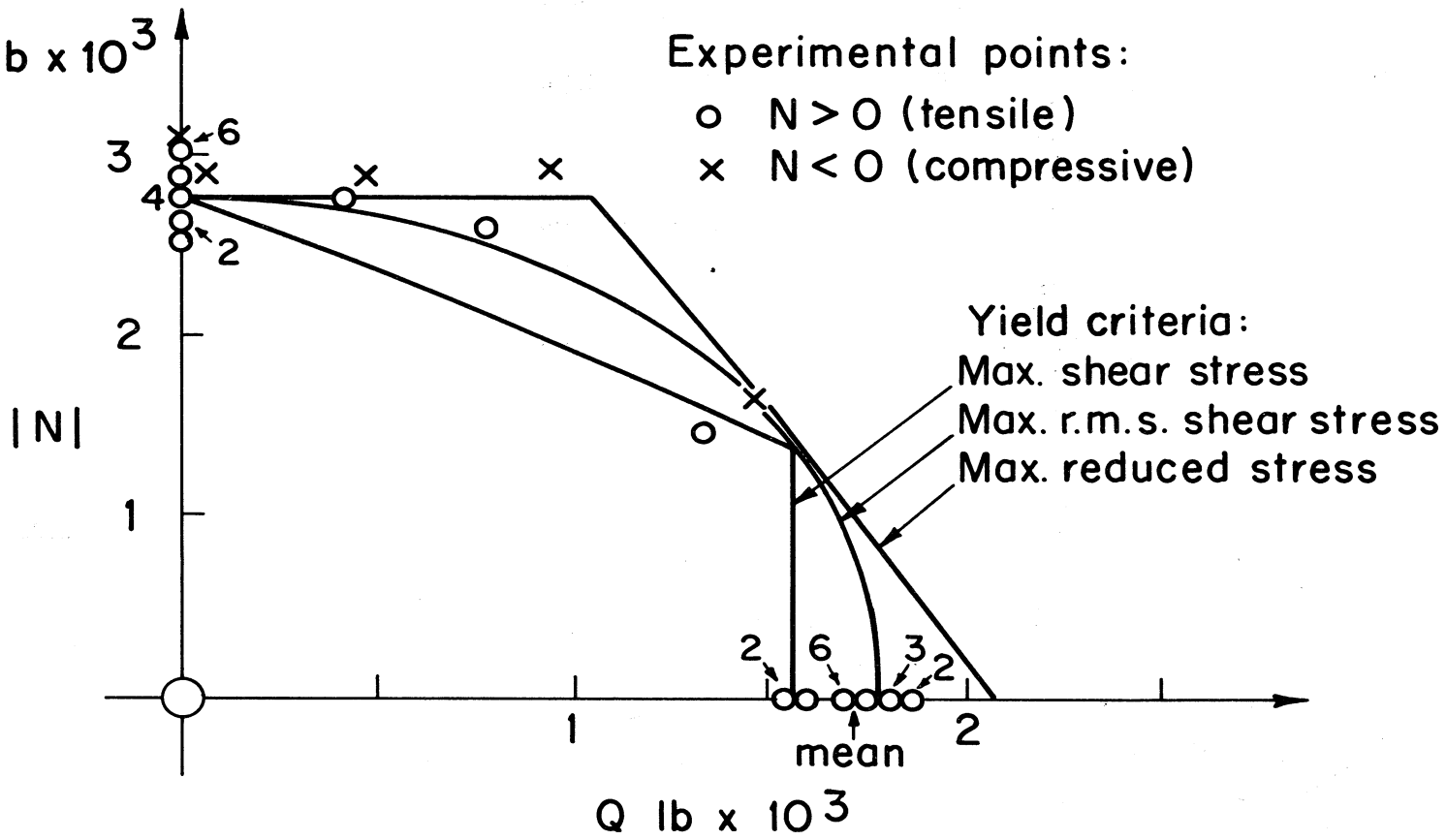

Fig. 10. Normalized SAE 1045 steel: Initial loadings which induced a plastic effective strain of .003. The curves showing the values expected on the basis of three alternative yield criteria have been scaled to pass through the mean of the fourteen tests carried out with axial force only (Q = 0).

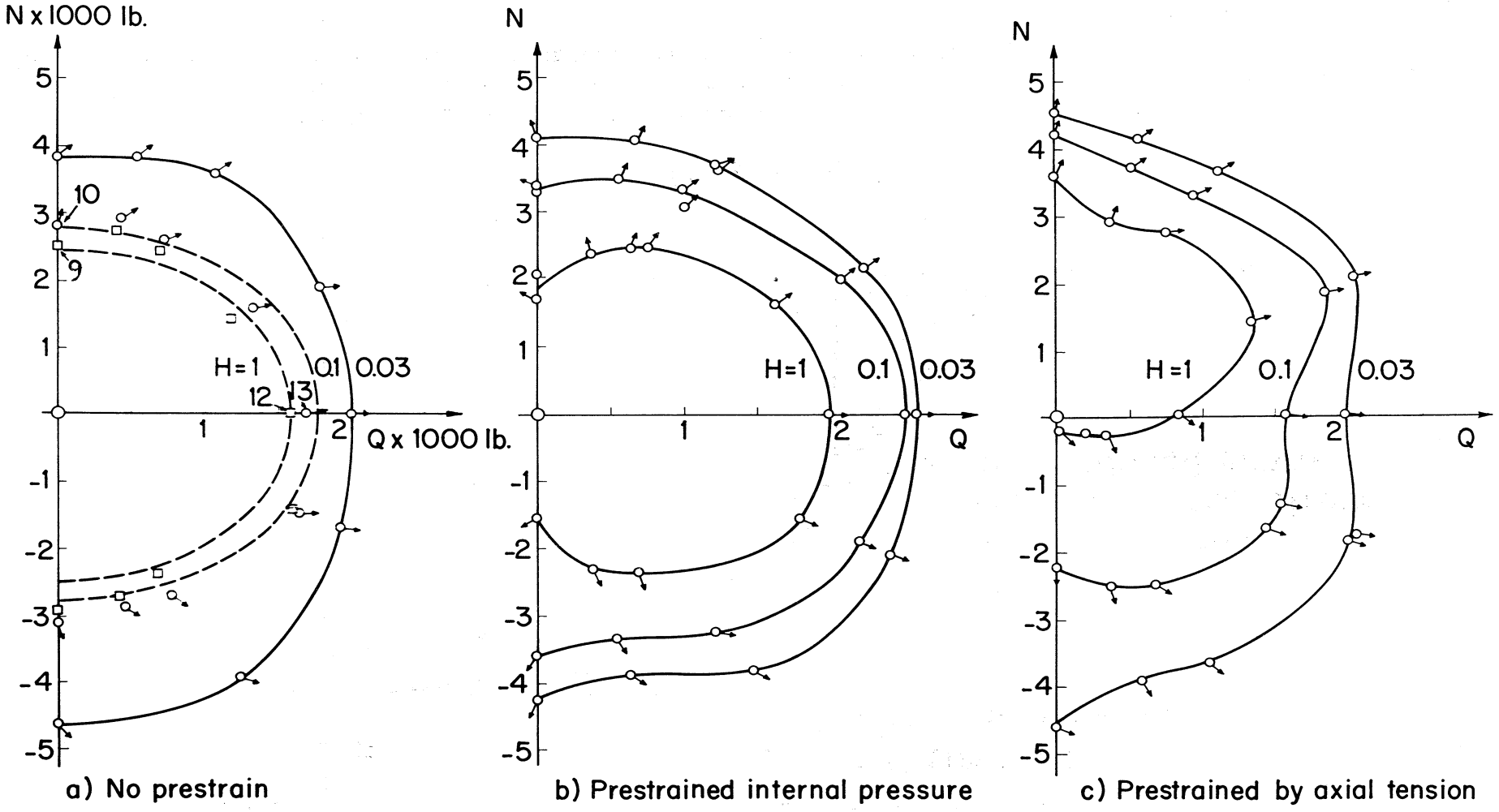

Fig. 11. Normalized SAE 1045 steel: Influence of prestrain on strain hardening characteristics. Plastic effective strain during prestrain: 0.03.

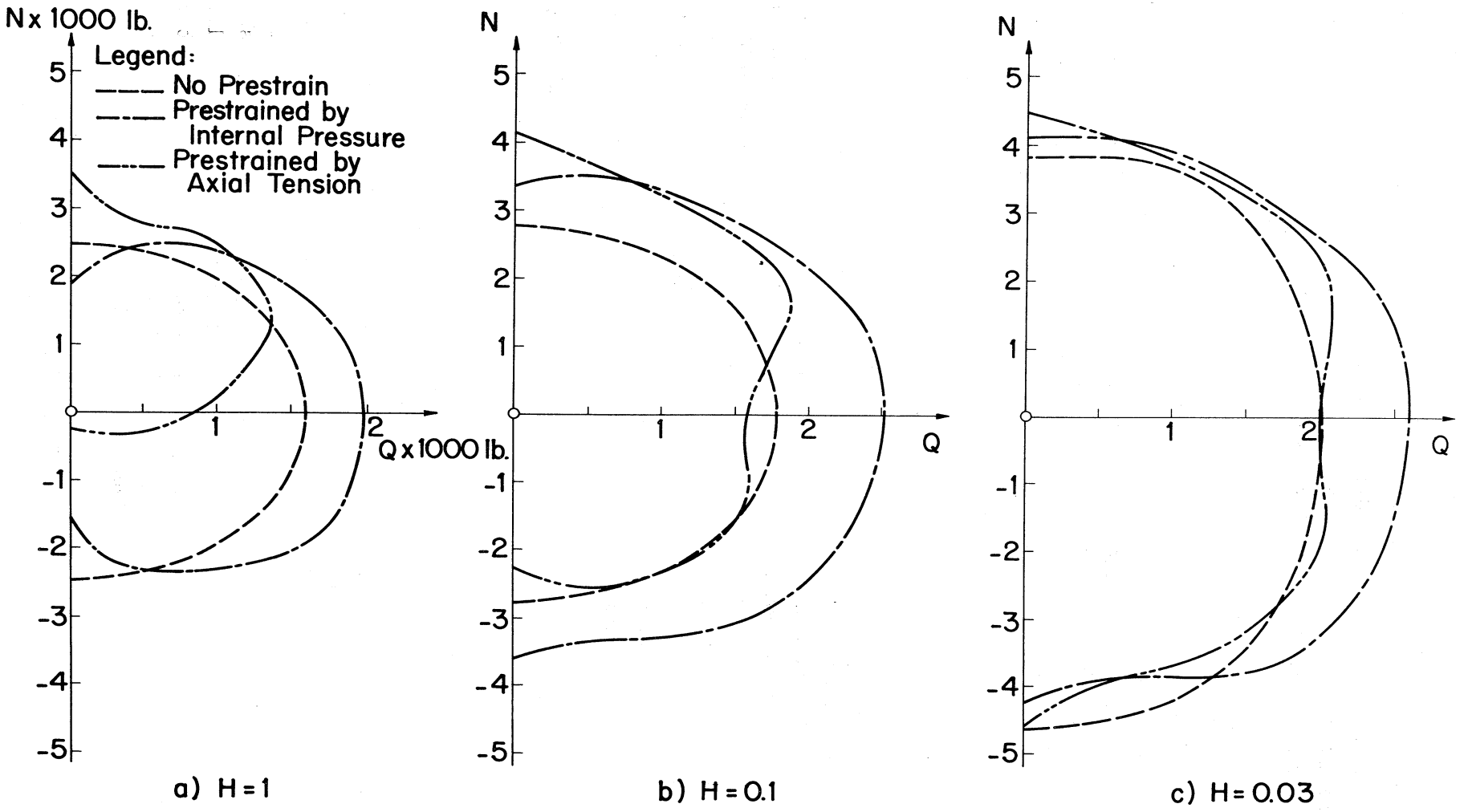

Fig. 12. Normalized SAE 1045 steel: Comparison of effects of prestrain at various hardening levels.

Figures 11b and 11c show contours of constant hardening rate for specimens that were prestrained by internal pressure (N = 0) and axial tension (Q = 0), respectively. At the higher values of H (reached first), there is a distinct shift of the contours towards the direction of the prestrain—to the right in Fig. 11b and upwards in Fig. 11c. As strain progresses, the contours become much more nearly symmetrical about the origin.

The curves shown in Fig. 11 have been replotted in Fig. 12 to facilitate comparison between the prestraining programs at each of the three hardening rates for which contours have been drawn. At H = 1, Fig. 12a, the contours are well separated, but as strain continues, they become closer together, although there remains a significant difference between the contours for the test with prestrain due to internal pressure and the other two sets. The overall picture would appear to be a progression from behavior which could be approximated by the model of kinematic hardening[39] towards behavior for which an isotropic hardening model would be more suitable. The symmetry of Fig. 12c about the Q axis is quite remarkable in view of the radically different prestraining programs.

The short arrows in Fig. 11 show the directions of the (generalized) strain rate increments at various levels of hardening. If the hardening rate contours can be interpreted as yield surfaces for the purposes of plastic theory, then these arrows should point in the direction of the outwards drawn normal to the contours. Inspection of Fig. 11 shows that the direction of the arrows is invariably outwards, and in many cases it lies close to the outwards drawn normal at the point concerned. The changes in direction of the arrows along the N axis in Fig. 11b is of particular interest; one might infer that the larger contours extend considerably in the half plane where Q is negative, which lends further support to the concept that the significant plastic flow property of the material might be simulated by an isotropic model at large plastic strain levels.

FRACTURE

It was of some interest to note whether there was any consistent visible evidence of the load history in the nature of the fracture surfaces. This turned out not to be the case, and is further evidence of the minor long term effects due to single overloads being in unusual stress directions. Figure 13 shows typical fracture surfaces. Photographs on the left in Fig. 13, show tubes in which the traction ratio was held constant throughout the loading, while those in the center and on the right were subject to one of the two prestraining programs. There was no apparent difference in the appearance of the fractures in the tubes which had been prestrained.

The type of fracture shown in the upper photographs was also typical of all tubes tested at higher ratios of N/Q, while the type shown in the lower

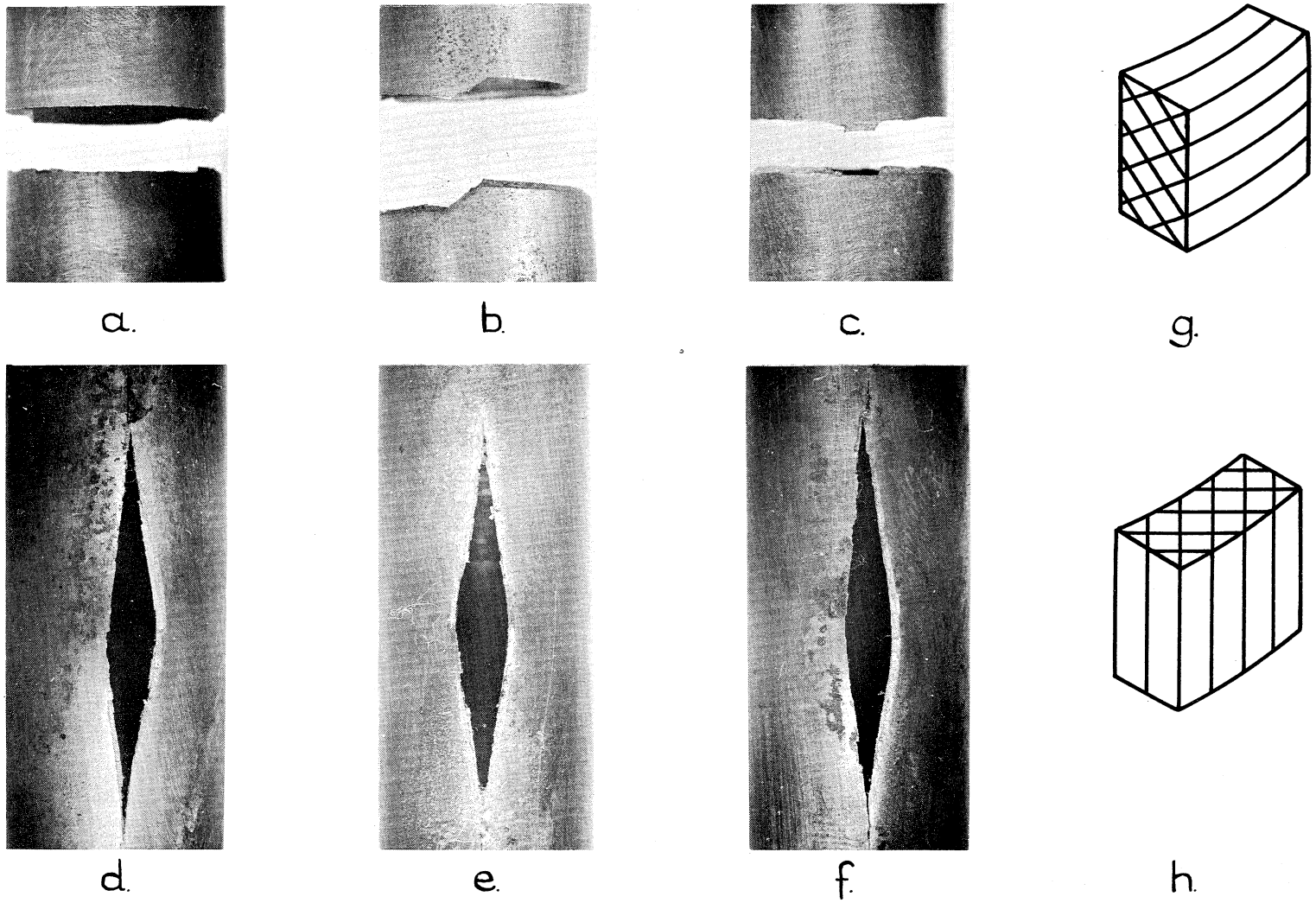

Fig. 13. Appearance of tube fractures. The top photographs show specimens fractured with the traction ratio held at N/Q = 3, (a) throughout the loading, (b) after tensile prestrain and (c) after prestrain by internal pressure. The lower photographs (d), (e), (f) show the corresponding cases for the traction ratio N/Q = 1. Possible slip plane patterns for the upper and lower photographs are shown in (g) and (h) respectively.

photographs was typical for the lower ratios. At a traction ratio $N/Q = -1$ and below, local or general buckling occurred and no information was obtained.

In Fig. 13, the photographs were selected to illustrate the transition between the two modes of fracture. Reference to Fig. 11, and the analysis in Part I reveals that this transition occurs at the traction ratio when, in the analysis for the maximum shear stress criterion, σ_z replaces σ_θ as the intermediate principal stress in much of the cross section. If slip along the lines of maximum shearing stress were to prove most damaging and lead to eventual cleavage on these planes, then the planes would be expected to follow the patterns shown in (g) and (h) of Fig. 13. The pattern (g) would occur when σ_θ was the intermediate stress and (h) would occur when it was replaced by σ_z. These slip patterns are highly suggestive of the actual cleavage patterns shown in the photographs.

The testing of a relatively large number of specimens to fracture after a prestraining program presented an opportunity to look for possible effects on ductility. Figure 14 shows a comparison between the subsequent strains at 0.95 the failure load and the strains at 0.95 the failure load in unprestrained specimens.

The strains ϵ_z, ϵ_θ are those observed at the outer surface. The radial strain ϵ_r has been computed assuming zero dilation for the plastic strain component. The data shows considerable scatter and the lines that have been drawn are intended to indicate possible trends only. Strains in the θ and z directions are by no means equal, and the particular geometry of the tube must be playing a significant role. Evidently it would be unjustified, in view of the possibilities for local or general instability, to assume that equivalent ductility would necessarily be achieved in a structure of different shape that might be of practical interest. However, the relative reductions in ductility due to prestrain which are evident in the trend lines may well have qualitative significance. The pattern is not unexpected. The simple shear prestrain, Fig. 14a, is a high proportion of the "available" strain and subsequent ductility is significantly reduced, although still adequate to allow the redistribution of forces which must remain possible if ultimate strength theories for carrying capacity are to be employed. On the other hand, the tensile prestrain, Fig. 14b, was much smaller in relation to the "available" strain, and the subsequent ductility appears to be relatively unaffected.

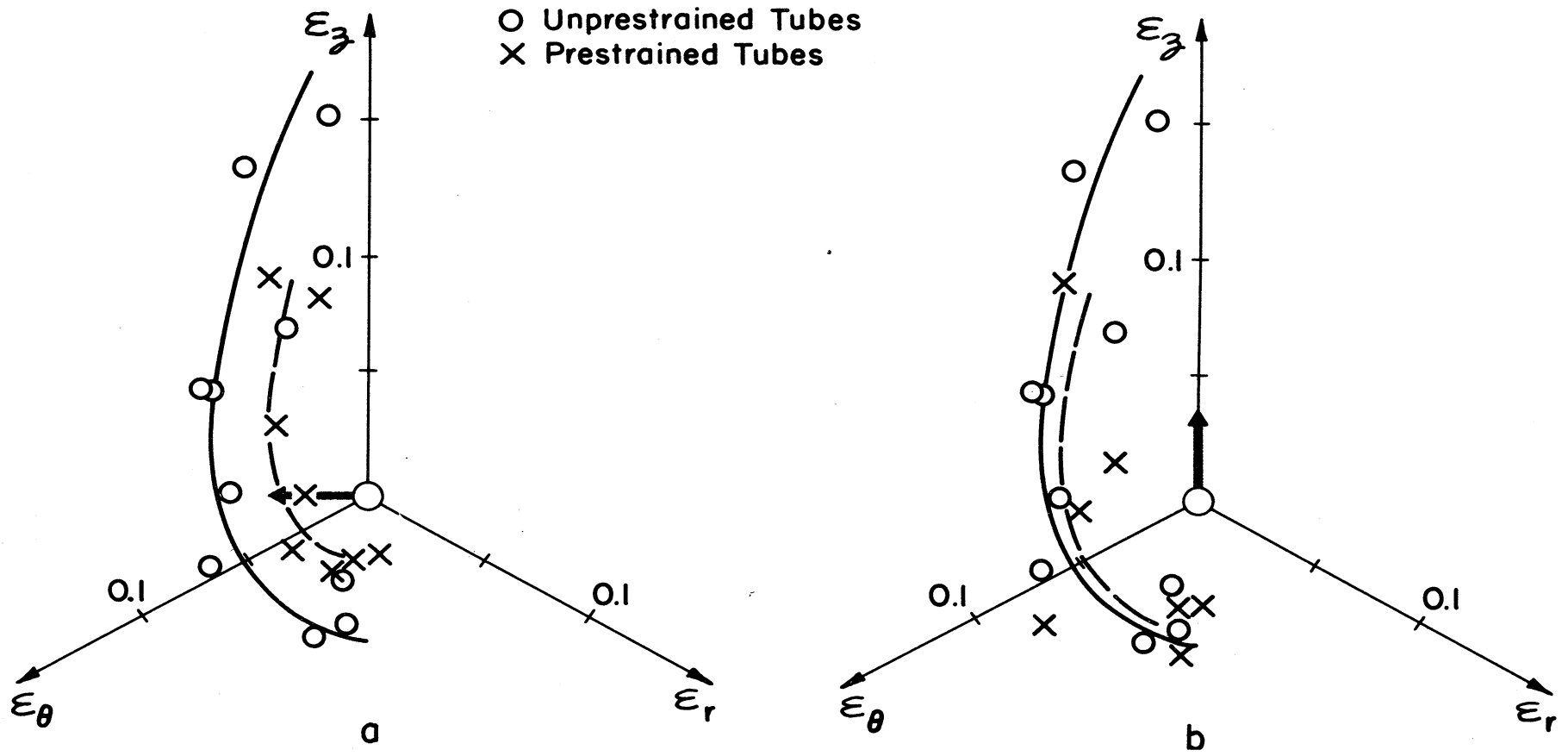

Fig. 14. Effect of prestraining on the plastic strain reached at 0.95 the fracture/instability load (a) after prestrain due to internal pressure only (N = 0) and (b) after prestrain due to axial tension only (Q = 0). The amount and directions of the plastic prestrain ($\bar{\varepsilon}^p$ = .03) are indicated by the thick arrows at the origins.

3. IMPLICATIONS FOR DESIGN

Some questions were posed in the Introduction concerning the influence of prior plastic deformation as it might concern the designer and it would, perhaps, be worthwhile to review the results of the investigation from that point of view.

It has been found that ductility can remain unaffected even by large prestrains if applied only once. The data (Fig. 14) shows considerable scatter, but it is clear that very large reserves of ductility remain whatever the nature of the subsequent stress system. This result has been established for two radically different prestrain systems, due to simple tension and simple shear, and it is reasonable to conclude similar results would be obtained if intermediate prestrain systems were used. It follows that a single overload would have to be very high indeed to reduce the metal to the state where there was insufficient ductility to allow the redistribution of stress associated with plastic yielding to take place prior to fracture. There seems to be scope for ultimate strength design even in heavily overstrained material.

The selection of a suitable mathematical model for a strain hardening material has always presented a serious problem to designers. In this investigation, we have shown that the surfaces of constant hardening rate do probably retain the properties of convexity and of normality of the strain rate increment vectors with sufficient accuracy to enable them to be treated as yield surfaces for successive ideally plastic models of the material. Although in the early stages of subsequent deformation the effective yield surfaces are displaced by prior straining (Fig. 12a) and analysis becomes difficult due to the presence of anisotropy, the later behavior becomes more and more symmetric and a fully isotropic model might well be adequate for the purposes of plastic analyses. This conclusion does not apply to elastic analysis of prestrained material. Proof strengths based on the curves shown in Fig. 12a would have to be used and the analysis is unlikely to reflect accurately available load carrying capacity of the component.

The contours of constant hardening rate are plotted in traction space because of the difficulties inherent in interpreting the tractions in terms of stresses for the tube test (see Part I); however the conclusions regarding approximate convexity of the contours and the normality of strain rate vectors, once established in traction space, are also valid in a stress space. The choice of yield criterion (expressed in terms of stresses) can be made in a perfectly logical fashion by comparing the test data with the curves in traction space computed for the various yield criteria in Part I of the report.

The conclusions reached in this Part of the report apply in the strictest sense only to the material as tested; however they may be indicative of the be-

havior of a broad class of materials. The precise range must await further programs of testing within the framework laid down in the current investigation.

REFERENCES

1. Haythornthwaite, R. M., "Range of Yield Condition in Ideal Plasticity," Proc. Am. Soc. Civil Engineers, Vol. 87, No. EM6, 1961, pp. 117-133. See also Trans. Am. Soc. Civil Engineers, Vol. 127, Part I, 1962, pp. 1252-1268.

2. Tresca, M., "Mémoire sur le Poinçonnage des Metaux," Mémoires des Savents Etrangers, Acad. Sci. (Paris) Vol. 20, 1869, pp. 617-838.

3. Saint-Venant, B. de, "Sur l'Intensité des Forces Capables de Déformer, avec Continuité, des Blocs Ductiles, Cylindriques, Pleins ou Évidés, et Placés dans Diverses Circonstances," Comptes Rendus, Acad, Sci. (Paris), Vol. 74, 1872, pp. 1009-1015.

4. Saint-Venant, B. de, "Sur un Complément à Donner à une des Équations Presentées par M. Levy pour les Mouvements Plastiques qui sont Symétriques autour d'un même Axe," Comptes Rendus, Acad. Sci. (Paris), Vol. 74, 1872, pp. 1083-1087.

5. Turner. L. B., "The Stresses in a Thick Hollow Cylinder Subjected to Internal Pressure," Trans. Cambridge Phil. Soc., Vol. 21, No. 14, 1910, pp. 377-396.

6. Macrae, A. E., "Overstrain in Metals and its Application to the Autofrettage Process of Cylinder and Gun Construction," H.M.S.O., London, 1930.

7. Nadai, A., "On the Mechanics of the Plastic State of Metals," Trans. Am. Soc. Mechanical Engineers, Vol. 52, Sec. APM, 1930, pp. 193-216.

8. Cook, G., "The Stresses in Thick-walled Cylinders of Mild Steel Overstrained by Internal Pressure," Proc. Instn. Mechanical Engineers, Vol. 126, 1934, pp. 407-461.

9. Beliaev, N. M. and Sinitski, H. K., "Stresses and Strains in Thick Walled Cylinders in the Elastic-Plastic State," Izvestia, Acad. Sci. U.S.S.R., Vol. 2, 1938, pp. 3-54.

10. Jeansen, C. F., "A Treatise on the Radial Expansion of Guns," U.S. Navy Bureau of Ordnance, Washington, 1938.

11. Manning, W.R.D., "The Overstrain of Tubes by Internal Pressure," Engineering, Vol. 159, 1945, pp. 101-102 and pp. 183-184.

12. Sokolovsky, V. V., "Theory of Plasticity," Moscow, 1946, Ch. 3.

13. Hill, R., Lee, E. H., and Tupper, S. J., "The Theory of Combined Plastic and Elastic Deformation with Particular Reference to a Thick Tube under Internal Pressure," Proc. Roy. Soc., London, Ser. A 191, 1947, pp. 278-303.

14. McGregor, C. W., Coffin, L. F. Jr., and Fisher, J. C., "Partly Plastic Thick Walled Tubes," J. Franklin Inst., Vol. 245, 1948, pp. 135-158.

15. Hodge, P. G. Jr., and White, G. N. Jr., "A Quantitative Comparison of Flow and Deformation Theories of Plasticity," J. Appl. Mech., Vol. 17, 1950, pp. 180-184.

16. Allan, D. N. de G., and Sopwith, D. G., "The Stresses and Strains in a Partially Plastic Thick Tube under Internal Pressure and End Load," Proc. Roy. Soc. London Ser. A, 205, 1951, pp. 69-83.

17. Steele, M. C., "Partially Plastic Thick-walled Cylinder Theory," Trans. Am. Soc. Mechanical Engineers, Vol. 74 (J. Appl. Mech. Vol. 19), 1952, pp. 133-140.

18. Koiter, W. T., "On Partially Plastic Thick Walled Tubes," in Anniversary Volume on Applied Mechanics dedicated to C. B. Biezeno, H. Stam., Haarlem, 1953, pp. 232-251.

19. Bland, D. R., "Elastoplastic Thick-walled Tubes of Work-hardening Material Subject to Internal and External Pressures and to Temperature Gradients," J. Mech. Phys. Solids, Vol. 4, 1956, pp. 209-229.

20. Rzhanitsyn, A. R., "Plastic Deformations of a Tube under Axially Symmetric Load," Izvestia, OTN, Acad. Sci., U.S.S.R., 1958, pp. 60-65.

21. Crossland, B. and Bones, J. A., "The Ultimate Strength of Thick-walled Cylinders subjected to Internal Pressure," Engineering, Vol. 179, 1959, pp. 80-83, 114-117.

22. Weiner, J. H. and Huddleston, J. V., "Transient and Residual Stresses in Heat Treated Cylinders," Trans. Am. Soc. Mechanical Engineers, Ser. E, Vol. 81 (J. Appl. Mech. Vol. 26) 1959, pp. 31-39.

23. Kammash, T. B., Murch, S. A., and Naghdi, P. M., "The Elastic-plastic Cylinder Subjected to Radially Distributed Heat Source, Lateral Pressure and Axial Force with Application to Nuclear Reactor Fuel Elements," J. Mech. Phys. Solids, Vol. 8, 1960, pp. 1-25.

24. Becker, S. J., "An Analysis of the Yielded Compound Cylinder," Trans. Am. Soc. Mechanical Engineers, Ser. B, Vol. 83, 1961, pp. 43-49.

25. Panarelli, J. E. and Hodge, P.G. Jr., "Interaction of Pressure, End Load, and Twisting Moment for a Rigid-plastic Circular Tube," Trans. Am. Soc. Mechanical Engineers, Ser. E, Vol. 30 (J. Appl. Mech. Vol. 30) 1963, pp. 396-400.

26. Drucker, D. C., "Some Implications of Work Hardening and Ideal Plasticity," Quart. Appl. Math., Vol. 7, 1950, pp. 411-418.

27. Drucker, D. C., "A More Fundamental Approach to Plastic Stress-strain Relations," Proc. Ist. U.S. Nat. Congr. Applied Mechanics (1951), ASME, New York, 1952, pp. 487-491.

28. Shield, R. T., "On Plastic Flow of Metal under Conditions of Axial Symmetry," Proc. Roy. Soc. London Ser. A 233, 1955, pp. 267-286.

29. Koiter, W. T., "Stress-strain Relations, Uniqueness and Variational Theorems for Elastic-plastic Materials with a Singular Yield Surface," Quart. Appl. Math., Vol. 11, 1953, p. 350.

30. Haythornthwaite, R. M., "Mechanics of the Triaxial Test for Soils," Proc. Am. Soc. Civil Engineers, Vol. 86, SM5, 1960, pp. 35-62.

31. Naghdi, P. M., Essenberg, F. and Koff, W., "An Experimental Study of Initial and Subsequent Yield Surfaces in Plasticity," J. Appl. Mech., Vol. 25, 1958, pp. 201-209.

32. Hu, L. W., and Bratt, J. F., "Effect of Tensile Plastic Deformation on Yield Condition," J. App. Mech. Vol. 25, 1958, p. 411.

33. Gill, S. S., and Parker, J., "Plastic Stress-strain Relationships—Some Experiments in the Effect of Loading Path and Loading History," J. Appl. Mech., Vol. 26, 1959, pp. 77-87.

34. Phillips, A., and Gray, G. A., "Experimental Investigation of Corners in the Yield Surface," J. Basic Engineering, Vol. 83, Ser. D, 1961.

35. Ivey, J., "Plastic Stress-strain Relations and Yield Surfaces for Aluminium Alloys," J. Mechanical Engineering Sci. Vol. 3, 1961, pp. 15-31.

36. Parker, J. and Bassett, M. B., "Plastic Stress-strain Relationships—Some Experiments to Derive a Subsequent Yield Surface," J. App. Mech., Vol. 31, 1964, pp. 676-682.

37. Jenkins, D. R., "Kinematic Hardening of Zinc Alloy Tubes," J. App. Mech., Vol. 32, 1965, pp. 849-858.

38. Jenkins, D. R., Gascoigne, H. E., Wolf, L. W. and Clark, S. K., "Effect of State of Stress on the Failure of Metals at Various Temperatures," Report 2797-9-F of The University of Michigan to U.S. Air Force, Wright Air Development Division, under contract AF 33(616)-6041, March 1960. (Also WADD Tech. Rpt. 60-234.)

39. Prager, W., "The Theory of Plasticity—A Survey of Recent Achievements," Proc. Inst. Mech. Eng., Vol. 41, 1955, pp. 3-19.

Unclassified
Security Classification

DOCUMENT CONTROL DATA - R&D

(Security classification of title, body of abstract and indexing annotation must be entered when the overall report is classified)

1. ORIGINATING ACTIVITY *(Corporate author)*
The University of Michigan, College of Engineering
Department of Engineering Mechanics
Ann Arbor, Michigan

2a. REPORT SECURITY CLASSIFICATION
Unclassified

2b. GROUP

3. REPORT TITLE

FLOW AND FRACTURE OF METALS UNDER COMPLEX STRESS

4. DESCRIPTIVE NOTES *(Type of report and inclusive dates)*
Final Summary Report, 3 March 1964—30 September 1965

5. AUTHOR(S) *(Last name, first name, initial)*

Haythornthwaite, R. M., Jenkins, D. R., Coon, M. D., Felber, C. K.

6. REPORT DATE	7a. TOTAL NO. OF PAGES	7b. NO. OF REFS
May 1966	40	39

8a. CONTRACT OR GRANT NO. AF 33(615)-1572

b. PROJECT NO. 7353

c. Task No. 735301

d.

9a. ORIGINATOR'S REPORT NUMBER(S)
06348-20-F

9b. OTHER REPORT NO(S) *(Any other numbers that may be assigned this report)*
AFML-TR-66-111

10. AVAILABILITY/LIMITATION NOTICES This document is subject to special export controls and each transmittal to foreign governments or foreign nationals may be made only with prior approval of the Metals and Ceramics Division, Air Force Materials Laboratory (MAMS), Wright-Patterson Air Force Base, Ohio 45433.

11. SUPPLEMENTARY NOTES

12. SPONSORING MILITARY ACTIVITY
Air Force Materials Laboratory, Research and Technology Division, Air Force Systems Command, Wright-Patterson AFB, Ohio

13. ABSTRACT The effects of severe initial prestrain on the response of a steel to complex stress states is investigated in a series of tube tests. The steel becomes highly anisotropic, with a pronounced Bauschinger effect, so far as the resumption of plastic flow is concerned. A detailed analysis of the subsequent history of hardening shows that, in the later stages of plastic flow, it may be possible to simulate the behavior of the material with reasonable accuracy by means of an isotropic rigid-plastic model. Even after substantial prestrains (plastic effective strain, 0.03) sufficient ductility remains to allow the redistribution of loads necessary for an ultimate strength (plastic) analysis of components. In Part I of the report a relatively complete study is made on the basis of plastic theory and it is shown that the stress distribution may be highly nonuniform even in a very thin cylinder; moreover the distribution is dependent on the nature of the yield criterion and so cannot be known in advance. This circumstance renders the calculation of "average" stresses of limited value and it is better to deal directly with the applied tractions, a procedure which is adopted in the remainder of the report. Part II presents details of the series of tests on tubes subject to various combinations of internal pressure and a tensile or compressive axial load.

DD FORM 1 JAN 64 1473

Unclassified
Security Classification

14. KEY WORDS	LINK A		LINK B		LINK C	
	ROLE	WT	ROLE	WT	ROLE	WT
Metals Complex stress Prestraining Steel tubes Ductility Fracture Plasticity Yield criteria						

INSTRUCTIONS

1. ORIGINATING ACTIVITY: Enter the name and address of the contractor, subcontractor, grantee, Department of Defense activity or other organization *(corporate author)* issuing the report.

2*a*. REPORT SECURITY CLASSIFICATION: Enter the overall security classification of the report. Indicate whether "Restricted Data" is included. Marking is to be in accordance with appropriate security regulations.

2*b*. GROUP: Automatic downgrading is specified in DoD Directive 5200.10 and Armed Forces Industrial Manual. Enter the group number. Also, when applicable, show that optional markings have been used for Group 3 and Group 4 as authorized.

3. REPORT TITLE: Enter the complete report title in all capital letters. Titles in all cases should be unclassified. If a meaningful title cannot be selected without classification, show title classification in all capitals in parenthesis immediately following the title.

4. DESCRIPTIVE NOTES: If appropriate, enter the type of report, e.g., interim, progress, summary, annual, or final. Give the inclusive dates when a specific reporting period is covered.

5. AUTHOR(S): Enter the name(s) of author(s) as shown on or in the report. Enter last name, first name, middle initial. If military, show rank and branch of service. The name of the principal author is an absolute minimum requirement.

6. REPORT DATE: Enter the date of the report as day, month, year; or month, year. If more than one date appears on the report, use date of publication.

7*a*. TOTAL NUMBER OF PAGES: The total page count should follow normal pagination procedures, i.e., enter the number of pages containing information.

7*b*. NUMBER OF REFERENCES: Enter the total number of references cited in the report.

8*a*. CONTRACT OR GRANT NUMBER: If appropriate, enter the applicable number of the contract or grant under which the report was written.

8*b*, 8*c*, & 8*d*. PROJECT NUMBER: Enter the appropriate military department identification, such as project number, subproject number, system numbers, task number, etc.

9*a*. ORIGINATOR'S REPORT NUMBER(S): Enter the official report number by which the document will be identified and controlled by the originating activity. This number must be unique to this report.

9*b*. OTHER REPORT NUMBER(S): If the report has been assigned any other report numbers *(either by the originator or by the sponsor)*, also enter this number(s).

10. AVAILABILITY/LIMITATION NOTICES: Enter any limitations on further dissemination of the report, other than those imposed by security classification, using standard statements such as:

(1) "Qualified requesters may obtain copies of this report from DDC."

(2) "Foreign announcement and dissemination of this report by DDC is not authorized."

(3) "U. S. Government agencies may obtain copies of this report directly from DDC. Other qualified DDC users shall request through _____."

(4) "U. S. military agencies may obtain copies of this report directly from DDC. Other qualified users shall request through _____."

(5) "All distribution of this report is controlled. Qualified DDC users shall request through _____."

If the report has been furnished to the Office of Technical Services, Department of Commerce, for sale to the public, indicate this fact and enter the price, if known.

11. SUPPLEMENTARY NOTES: Use for additional explanatory notes.

12. SPONSORING MILITARY ACTIVITY: Enter the name of the departmental project office or laboratory sponsoring *(paying for)* the research and development. Include address.

13. ABSTRACT: Enter an abstract giving a brief and factual summary of the document indicative of the report, even though it may also appear elsewhere in the body of the technical report. If additional space is required, a continuation sheet shall be attached.

It is highly desirable that the abstract of classified reports be unclassified. Each paragraph of the abstract shall end with an indication of the military security classification of the information in the paragraph, represented as *(TS), (S), (C), or (U)*.

There is no limitation on the length of the abstract. However, the suggested length is from 150 to 225 words.

14. KEY WORDS: Key words are technically meaningful terms or short phrases that characterize a report and may be used as index entries for cataloging the report. Key words must be selected so that no security classification is required. Identifiers, such as equipment model designation, trade name, military project code name, geographic location, may be used as key words but will be followed by an indication of technical context. The assignment of links, rules, and weights is optional.